國 立 交 通 大 學

材料科學與工程系所

碩 士 論 文

具有高介電質閘極氧化層(二氧化鉿、氧化鑭)之

三五族金氧半電容其電性提升之研究

Study of Performance Improvement for

High-κ (HfO_2, La_2O_3)/III-V

Metal-Oxide-Semiconductor Capacitors

研 究 生：盧柏菁

指導教授：張　翼 博士

中 華 民 國 九 十 九 年 九 月

具有高介電質閘極氧化層(二氧化鉿、氧化鑭)之

三五族金氧半電容其電性提升之研究

Study of Performance Improvement for High-κ (HfO_2, La_2O_3)/III-V Metal-Oxide-Semiconductor Capacitors

研 究 生：盧柏菁　　Student：Po-Ching Lu

指導教授：張　翼 博士　　Advisor：Dr. Edward Yi Chang

國 立 交 通 大 學

材料科學與工程系所

碩 士 論 文

A Thesis

Submitted to Department of Materials Science and Engineering

College of Engineering

National Chiao Tung University

in partial Fulfillment of the Requirements

for the Degree of

Master

in

Materials Science and Engineering

September 2010

Hsinchu, Taiwan, Republic of China

中華民國九十九年九月

具有高介電質閘極氧化層(二氧化鉿、氧化鑭)之三五族金氧半電容其電性提升之研究

研究生：盧柏菁　　　　　　　　　　　　　　　　指導教授：張 翼 博士

國立交通大學材料科學與工程系所

摘要

傳統的互補式金氧半場效電晶體將在此世代遇到發展的瓶頸，而為了延續發展以及提升元件的特性，結合高介電質材料與高載子遷移率三五族半導體的研究逐漸受到重視。由於擁有極佳的載子傳輸特性，三五族復合物半導體將是未來通道材料的首選，因其擁有高速及低操作偏壓的元件特性。而採用高介電質材料作為閘極介電層是為了要抑制因元件尺寸的微縮所造成嚴重的閘極漏電流。然而高介電質材料與三五族半導體之間的界面問題始終阻礙著三五族金氧半元件的發展。本論文主要是利用分子束磊晶機台來沉積高品質的高介電質材料(二氧化鉿、氧化鑭)於三五族複合物半導體基板上來製備金氧半電容，並尋求各種可行的方法來改善介面品質以提升元件特性。

由本實驗結果顯示，二氧化鉿與砷化銦之間的界面品質可藉由較高的退火溫度來改善，而元件特性也隨之提升。然而，當退火溫度高於500℃，銦原子會由基板擴散至二氧化鉿，在界面有大量的氧化銦產生，導致元件特性因此變差。同時也研究出具有高介電常數的氧化鑭與砷化銦鎵之間有劇烈的交互作用，因此無法獲得低缺陷的界面品質。藉由嵌入一層熱穩定的二氧化鉿形成層狀堆疊的閘極介電層可改善介面問題並提升元件的電容值，並在具有高銦含量的電容上顯示出明顯的載子反轉行為。最後，兩階段退火處理對於元件特性的影響也同時被研究，而結果顯示出兩階段退火更能顯著的降低表面缺陷密度且獲得品質較佳的閘極氧化層。

Study of Performance Improvement for High-κ (HfO_2, La_2O_3)/III-V Metal-Oxide-Semiconductor Capacitors

Student：Po-Ching Lu **Advisor：Dr. Edward Y. Chang**

Department of Materials Science and Engineering
National Chiao Tung University

Abstract

To extent the limit of traditional Si-based MOS-devices, high-mobility channel materials and high dielectric constant (high-κ) materials as gate dielectrics for CMOS have been extensively studied. $In_XGa_{1-X}As$-channel has attracted much attention due to the much superior carrier mobility, especially electron mobility, than Si. Among many high-κ dielectric materials, HfO_2 is more attractive than other high-κ materials in terms of its high dielectric constant (κ~20-25), large energy band gap (~6eV), and thermally stable on III-V materials. Furthermore, rare-earth oxides (REOs) possess high dielectric constant and are expected to be used as gate dielectric materials for post-HfO_2 oxide era. However, the lack of high quality oxide/III-V semiconductor interface, especially REOs, is the main obstacle for the development for III-V MOSFETs.

In this thesis, molecular beam epitaxy (MBE) was used to deposit high quality high-κ thin films on III-V MOS-capacitors. Post deposition annealing (PDA) was performed after the gate oxide deposition and optimized to improve the device performance. The MOS-capacitor after the 500°C PDA annealing demonstrated the lowest interface trap density (D_{it}) value due to the reduction of

native oxide (As_2O_3). However, as the annealing temperature approached 550 ^oC, a large number of indium (In) atoms diffused into the HfO_2 layer with the increase of InO_X and In_2O_3 formation so that the device performance was degraded.

Inserting a thin interlayer (IL) between REO and III-V channel can prevent their inter-reaction and enhance the capacitance value. The capacitance enhance in the accumulation region due to the addition of La_2O_3 as compared to pure $HfO_2/In_XGa_{1-X}As$ MOS-capacitor from 0.73 ($\mu F/cm^2$) to 1.26 ($\mu F/cm^2$) for n-InAs capacitor, and from 0.5 ($\mu F/cm^2$) to 1.05 ($\mu F/cm^2$) for p-$In_{0.7}Ga_{0.3}As$ capacitor.

The two-steps annealing is a useful thermal treatment to obtain a low D_{it} and a small hysteresis value. The *C-V* characteristics would be improved after the second annealing with the small frequency dispersion. The experiment results also showed that a large temperature difference between the first step and the second step would cause the more serious hysteresis effect due to a large lattice mismatch between the two oxide layers.

致謝

兩年的時光匆匆而過，在不斷的失敗中學習成長，在冗長的實驗中磨練堅定的信念，最後能順利完成碩士論文，心裡的感動是難以言喻。

在這段時間裡，深受許多人的幫助與鼓勵。首先必須對指導教授張翼教授表達深深地感謝之意，感謝老師在實驗上提供了豐富的研究資源與儀器設備，以及在學問上給予我熱心的指教。再來要感謝我的指導學長林岳欽博士，短短兩年的碩士班期間，在實驗中一直悉心給予我指導與勉勵，沒有學長的協助與建議，是無法順利完成碩士學位。

另外還要感謝日本東京工業大學 Iwai 教授的協助，讓我有機會獲得高品質的閘極氧化層薄膜。此外也要感謝國家奈米元件實驗室(NDL)的工程師以及交大奈米中心(NFC)，同時提供優良的儀器設備與環境，使實驗能順利完成。

感謝 CSD Lab 的學長姐、同學、學弟妹以及秘書助理的協助幫忙與鼓勵，因為有你們的支持，讓我在面對挫折與困難時，更有堅定的信念與信心來面對，也因為有你們的陪伴，讓我兩年的碩士班生活是如此的多采多姿，在此，由衷的感謝你們，謝謝!

當然，我要特別感謝在我背後默默支持我的父母家人和女友，感謝你們在這段時間對我的包容、鼓勵與關心，讓我無後顧之憂，能專心一致的順利完成學業，你們的支持，是我堅持下去最大的動力。謝謝你們!

盧柏菁
2010.10.12

Contents

Abstract (Chinese) i

Abstract (English) ii

Acknowledgement iv

Contents v

Table Captions vii

Figure Captions viii

Chapter 1 Introduction 1

1.1 General Background 1

1.2 Thesis Content 3

Chapter 2 Overview of Metal-Oxide-Semiconductor Capacitors 5

2.1 The Theory of MOS-Capacitors 5

2.1.1 MOS-Capacitor with P-type Substrate 6

2.1.2 MOS-Capacitor with N-type Substrate 8

2.1.3 MOS-Capacitor Characterization 10

2.2 Requirements for Gate Dielectrics 12

2.3 High-κ Gate Materials 15

2.4 III-V Compound Semiconductors as Channel Materials 17

Chapter 3 Fabrication of III-V Metal-Oxide-Semiconductor Capacitors 18

3.1 Experimental Process Flow 18

3.2 Electron Beam Epitaxy (MBE) 19

Chapter 4 Fundamentals of Electrical Characteristics for III-V MOS-Capacitors **21**
4.1 Capacitance-Voltage (*C*-*V*) Characteristics 21
4.2 Leakage Current Density-Voltage (*J*-*V*) Characteristics 24
4.3 Interface Trap Density (D_{it}) by Conductance Method 24
Chapter 5 Experimental Results and Discussion **27**
5.1 Study on Electrical Characteristics of HfO_2/n-InAs Metal-Oxide-Semiconductor Capacitors with Different Post Deposition Annealing Temperatures 27
5.1.1 Introduction 27
5.1.2 Experiment 28
5.1.3 Results and Discussion 29
5.1.4 Conclusion 38
5.2 Performance Improved of Bilayer High-κ Gate Dielectrics for $In_XGa_{1-X}As$ Metal-Oxide-Semiconductor Capacitors 39
5.2.1 Introduction 39
5.2.2 Experiment 40
5.2.3 Results and Discussion 42
5.2.4 Conclusion 47
5.3 Effect of Thermal Treatment on Properties of HfO_2/p-$In_{0.7}Ga_{0.3}As$ Metal-Oxide-Semiconductor Capacitors 48
5.3.1 Introduction 48
5.3.2 Experiment 49
5.3.3 Results and Discussion 50
5.3.4 Conclusion 58
Chapter 6 Conclusion **59**
Reference **61**

Table Captions

Chapter 1

Table 1-1 Channel materials properties 4

Chapter 2

Table 2-1 Scaling down of MOSFETs by a scaling factor of k ….. 12

Table 2-2 Candidates for the metal, oxide of which has possibility to be used as high-κ gate insulator on periodic table 15

Table 2-3 Electron and hole mobility of various semiconductors 17

Chapter 5

Table 5-1-1 Comparison of electrical characteristics of the HfO_2/n-InAs capacitors at the different PDA temperatures 34

Table 5-1-2 Comparison of the Al_2O_3 and HfO_2/n-InAs MOS-capacitors 38

Table 5-3-1 Comparison of interface trap density (D_{it}) and hysteresis of the HfO_2/p-$In_{0.7}Ga_{0.3}As$ MOS-capacitors at the different first step PDA temperatures 51

Table 5-3-2 Comparison of interface trap density (D_{it}) and hysteresis of the HfO_2/p-$In_{0.7}Ga_{0.3}As$ MOS-capacitors with the first step annealing at 450°C and the different second step annealing temperatures 53

Table 5-3-3 Comparison of interface trap density (D_{it}) and hysteresis of the HfO_2/p-$In_{0.7}Ga_{0.3}As$ MOS-capacitors with the first step annealing at 500°C and the different second step annealing temperatures 56

Figure Captions

Chapter 1

Fig. 1-1 The trend of transistor technology 4

Fig. 1-2 Channel materials properties 4

Chapter 2

Fig. 2-1 Basic metal-oxide-semiconductor capacitor structure 5

Fig. 2-2 Band diagram of a MOS-capacitor with a p-type substrate 7

Fig. 2-3 Band diagram of a MOS-capacitor with a n-type substrate 9

Fig. 2-4 Band diagram of flat-band condition of a MOS-capacitor 10

Fig. 2-5 Concept of scaling rule 12

Fig. 2-6 Required physical gate length, equivalent oxide thickness (EOT) and supply voltage for the next 15 years reported on ITRS 2008 update 14

Fig. 2-7 Schematic illustration of gate leakage current under the different gate dielectrics of the MOS structure with (a) SiO_2 (b) High-κ 14

Fig. 2-8 Recent high-κ reports had been published in VLSI and IEDM symposium ... 16

Chapter 3

Fig. 3-1 Fabrication process flow of III-V MOS-capacitors 19

Fig. 3-2 Schematic of the MBE chamber for the deposition of high-κ gate materials..20

Chapter 4

Fig. 4-1 Cross-section and band diagram of a MOS-capacitor 23

Fig. 4-2 Capacitances of MOS-capacitors under the different bias conditions 23

Fig. 4-3 Equivalent circuit for conductance measurement (a) MOS-C with interface trap time constant $\tau_{it} = R_{it}C_{it}$, (b) simplified circuit of (a), (c) measured circuit 26

Chapter 5

Fig. 5-1-1 Structure of the HfO_2/n-InAs MOS-capacitor...29
Fig. 5-1-2 TEM images of interface (a) HfO_2/InAs, (b) HfO_2/$In_{0.53}Ga_{0.47}As$ 30
Fig. 5-1-3 *C-V* characteristics of the HfO_2/n-InAs MOS-capacitors after PDA at (a) 400°C (b) 450°C (c) 500°C (d) 550°C..32
Fig. 5-1-4 Bidirectional *C-V* sweeps of the HfO_2/n-InAs MOS-capacitors at the different PDA temperatures...34
Fig. 5-1-5 *XPS* spectra of the HfO_2/n-InAs MOS-capacitors at the different PDA temperatures 36
Fig. 5-1-6 *C-V* characteristics of the Al_2O_3/n-InAs MOS-capacitor 37
Fig. 5-2-1 Structures of the n-$In_XGa_{1-X}As$ MOS-capacitors..41
Fig. 5-2-2 Gate leakage current density, J_G-V_G, of La_2O_3, HfO_2, and La_2O_3/HfO_2 n-$In_{0.53}Ga_{0.47}As$ MOS-capacitors 42
Fig. 5-2-3 *C-V* characteristics of the n-$In_{0.53}Ga_{0.47}As$ MOS-capacitors with the different gate dielectrics (a) HfO_2 (b) La_2O_3 (c) La_2O_3/HfO_2 44
Fig. 5-2-4 *C-V* characteristics of the n-InAs MOS-capacitors with the different gate dielectrics (a) HfO_2 (b) La_2O_3/HfO_2..45
Fig. 5-2-5 Comparison of *C-V* characteristics at 100kHz of the La_2O_3/HfO_2 and HfO_2 $In_XGa_{1-X}As$ MOS-capacitors (a) n-InAs (b) p-$In_{0.7}Ga_{0.3}As$ 46
Fig. 5-3-1 Structure of the HfO_2/p-$In_{0.7}Ga_{0.3}As$ MOS-capacitor with the two-steps annealing process 50

Fig. 5-3-2 Comparison of interface trap density (D_{it}) and hysteresis of the HfO_2/p-$In_{0.7}Ga_{0.3}As$ MOS-capacitors at the different first step PDA temperatures 51
Fig. 5-3-3 Comparison of interface trap density (D_{it}) and hysteresis of the HfO_2/p-$In_{0.7}Ga_{0.3}As$ MOS-capacitors with the first step annealing at 450°C and the different second step annealing temperatures 53
Fig. 5-3-4 *C-V* characteristics of the HfO_2/p-$In_{0.7}Ga_{0.3}As$ MOS-capacitors with the first step annealing at 450°C and the different second step annealing temperatures 54
Fig. 5-3-5 Comparison of interface trap density (D_{it}) and hysteresis of the HfO_2/p-$In_{0.7}Ga_{0.3}As$ MOS-capacitors with the first step annealing at 500°C and the different second step annealing temperatures 56
Fig. 5-3-6 *C-V* characteristics of the HfO_2/p-$In_{0.7}Ga_{0.3}As$ MOS-capacitors with the first step annealing at 500°C and the different second step annealing temperatures 58

Chapter 1

Introduction

1.1 General Background

In the past few decades, continual scaling of conventional Si-based transistors following Moore's law is the main efforts for Si industry. The dimension will reach 22 nm node (10 nm gate length) in 2011, and most scientists believe this would be the terminal limitation for Si COMS [1-1]. Therefore, developing a new logic device technology becomes an essential issue. Candidates, which were always mentioned, included carbon nanotube (CNT) transistors, semiconductor nanowires, and spintronics Fig. 1-1 [1-2, 1-3]. But these technologies are still at a prototypical status.

III-V channel devices, especially III-V metal-oxide-semiconductor field-effect transistors (III-V MOSFETs), are of highly potential for the next generation logic devices due to their excellent performance. In general, III-V materials possess superior properties, including high carrier-mobility, high electron peak drift velocity even under high electrical field, and low electron effective mass, to allow logic devices operating much faster but at a lower power than modern Si devices. The detailed materials properties are listed in Table 1-1 and shown in Fig. 1-2. Recently, high indium (In) content $In_XGa_{1-X}As$-channel devices have been widely investigated due to the advantages of much higher carrier-mobility and the moderate energy band gap among III-V compound semiconductors [1-4~1-6], so $In_XGa_{1-X}As$ devices are

expected to have high potential for future beyond CMOS applications.

The major reason for the success for Si MOSFETs is that highly stable SiO_2/Si interface by thermal growing SiO_2 on Si. However, unlike SiO_2 on Si substrate, there are no stable native oxides on III-V compound semiconductors leading to the lack of high quality and high thermodynamically stable oxide/semiconductor interface, and it might cause serious Fermi-level pinning which degrades device performance. Moreover, it is hard to suppress the gate leakage current by an ultra-thin SiO_2 of downsizing transistors. Therefore, there have been a variety of efforts to solve the problems mentioned above. Recently, high-κ oxide materials introduced for gate dielectrics on III-V devices was one of the most promising methods to provide the high quality of dielectric/semiconductor interface [1-7]. Moreover, high-κ dielectrics possess high capacitance values which might enhance the performance of MOS devices under a low equivalent oxide thickness (EOT).

In this study, III-V MOS-capacitors which integrated the $In_XGa_{1-X}As$-channel with the high-κ gate dielectric were investigated. In order to exhibit the excellent performance of III-V MOS-capacitors, several approaches have been adopted. These efforts included that using the high indium (In) content $In_XGa_{1-X}As$-channel to enhance the carriers transport, obtaining high quality of high-κ gate dielectrics by the Molecular Beam Epitaxy (MBE) system, the bilayer gate dielectrics, and the thermal treatment to approach high performance of III-V MOS-capacitors.

1.2 Thesis Content

This thesis focuses on the study on the performance improvement of $In_XGa_{1-X}As$ metal-oxide-semiconductor capacitors (MOS-capacitors).

In chapter 2, the overview includes the basic operating mechanism of MOS-capacitors, and the performance of high-κ dielectrics and III-V high carrier-mobility channels are described. The detailed fabricating processes of the $In_XGa_{1-X}As$ MOS-capacitors are introduced in chapter 3. In chapter 4, the fundamentals of electrical characteristics of devices are described.

The experimental results and discussions are presented in chapter 5 and are divided into three parts. The first part discusses the effect of different post deposition annealing (PDA) temperatures on the electrical characteristics and the surface qualities of the HfO_2/n-InAs MOS-capacitors, the results are also compared to the Al_2O_3 capacitors. Due to the strong interaction between high-κ and III-V materials, high dielectric constant rare-earth oxides (REOs) are difficult to be used as gate dielectrics on III-V MOS-devices. Thus, inserting a thin HfO_2 interlayer (IL) between the rare-earth oxide and the III-V channel was tried and the results are discussed in the second part. The improvement of device performance by using the REO/HfO_2 bilayer gate dielectrics is also demonstrated. In the third part of chapter 5, the effects of thermal treatment of two-steps annealing process on the HfO_2/p-$In_{0.7}Ga_{0.3}As$ MOS-capacitors performance are studied. Finally, the conclusion of the thesis is given in chapter 6.

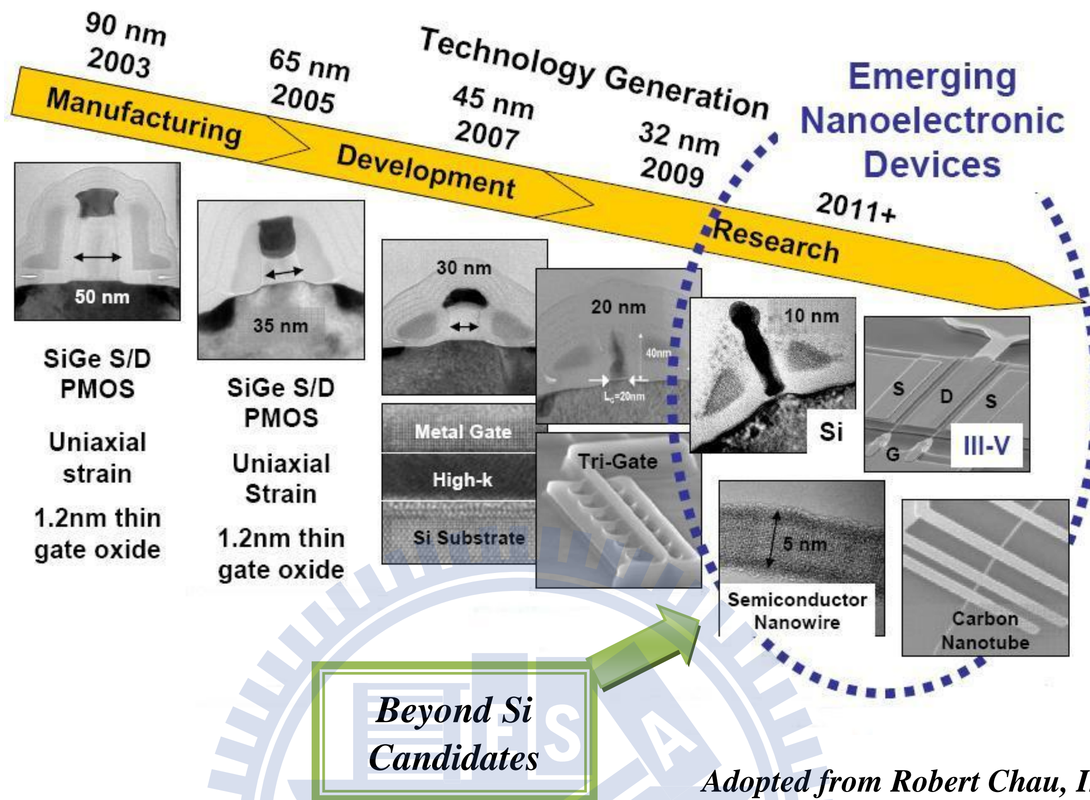

Fig. 1-1 The trend of transistor technology

Channel Material Properties at 295K

	Si	GaAs	$In_{.53}Ga_{.47}As$	InAs	InSb
Electron Mobility ($cm^2V^{-1}s^{-1}$ n_s=$1x10^{12}/cm^2$)	600	4,600	7,800	20,000	30,000
Electron Saturation Velocity (10^7 cm/s)	1.0	1.2	0.8	3.5	5.0
Ballistic Mean Free Path (nm)	28	80	106	194	226
Energy Band-gap	1.12	1.42	0.72	0.36	0.18

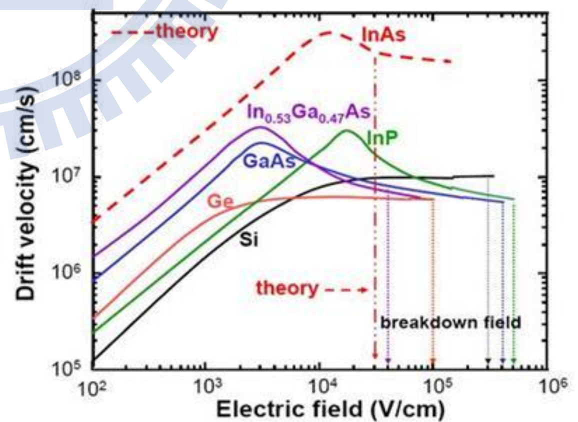

Table 1-1 & Fig. 1-2 Channel materials properties

Chapter 2

Overview of Metal-Oxide-Semiconductor Capacitors

2.1 The Theory of MOS-Capacitors [2-1]

Metal-Oxide-Semiconductor field-effect transistors (MOSFETs) are the most important devices which were used in digital integrated circuit applications today. In general, the major core of MOSFETs is Metal-Oxide-Semiconductor capacitors (MOSCAPs) which determine the device performance.

As shown in Fig. 2-1, a basic MOS-capacitor structure consists of, from bottom to top, the back side metal, the semiconductor substrate, a thin oxide layer, and the gate metal. Based on the type of the substrate, p-type or n-type, MOS-capacitors can be divided into two categories.

The main operation conditions of MOS-capacitors include accumulation, depletion, and inversion.

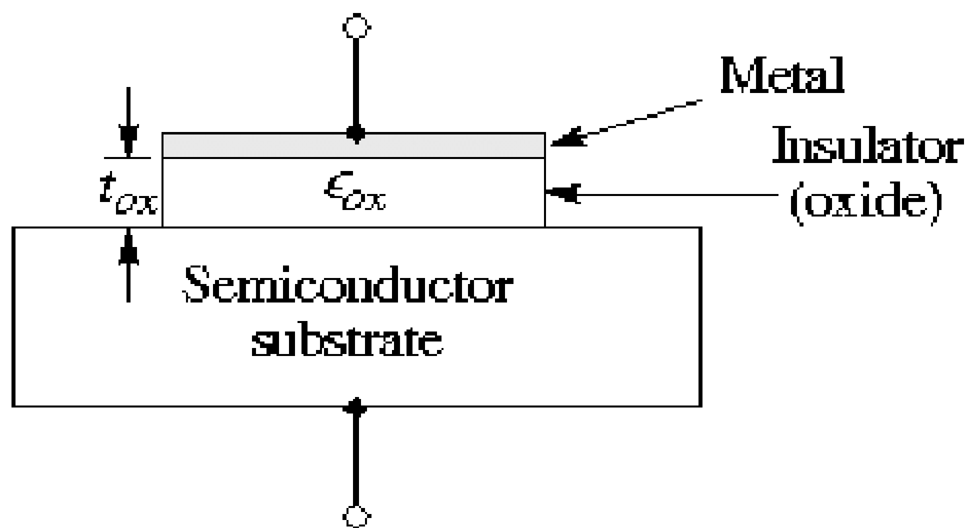

Fig. 2-1 Basic metal-oxide-semiconductor capacitor structure

2.1.1 MOS-Capacitor with P-type Substrate

Fig. 2-2 shows the band diagram of a MOS-capacitor with the p-type substrate. Under a negative gate voltage, the valence band at the oxide/semiconductor interface bent upward and could be close to the Fermi level, and it means that there is hole-accumulation at the semiconductor surface as shown in Fig. 2-2(a).

Under a small positive gate voltage, conduction band and intrinsic Fermi level bent downward and could be close to the Fermi level as shown in Fig. 2-2(b), and there is a depletion region occurs at the semiconductor surface. The depletion region expands with the increase of positive gate voltage.

As a much larger positive gate voltage is applied, the band bent even more as shown in Fig. 2-2(c). The intrinsic Fermi level at the interface is now lower than the Fermi level, so that it is n-type like at the oxide/semiconductor interface, which means the positive gate voltage starts to induce electrons at the interface. In this case, the amount of minority carriers (electrons) is greater than that of majority carriers (holes) leading to the formation of an inversion layer.

By applying a high enough positive gate voltage, the carriers on the p-type substrate surface are inverted from p (holes) to n (electrons), and it is called the NMOS-capacitors.

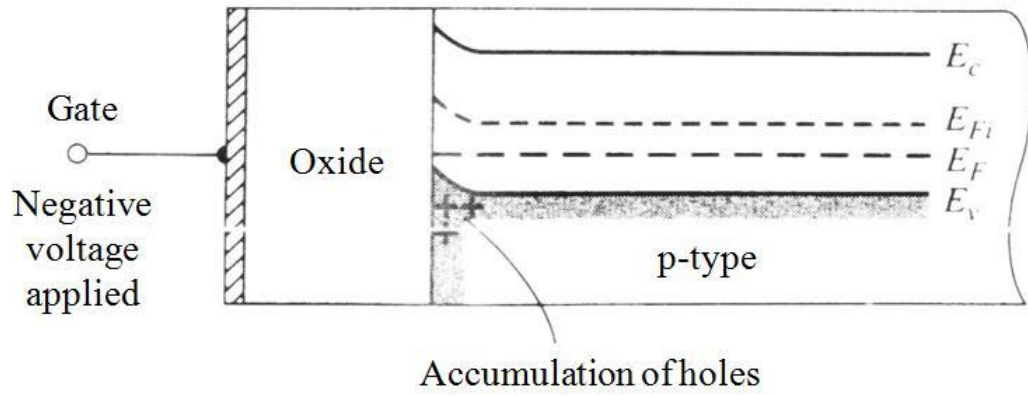

(a) Accumulation

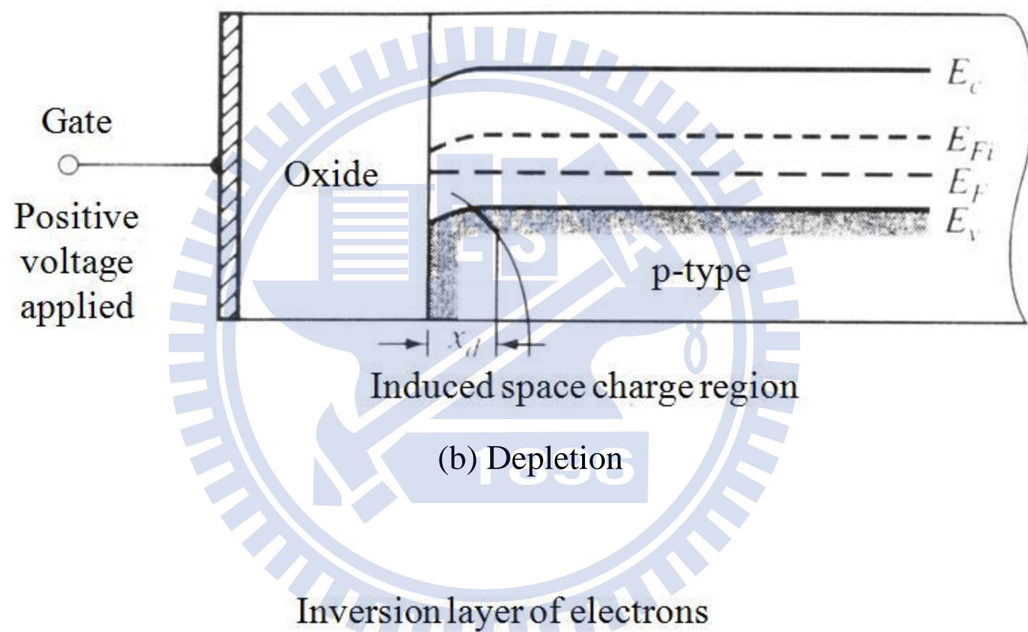

(b) Depletion

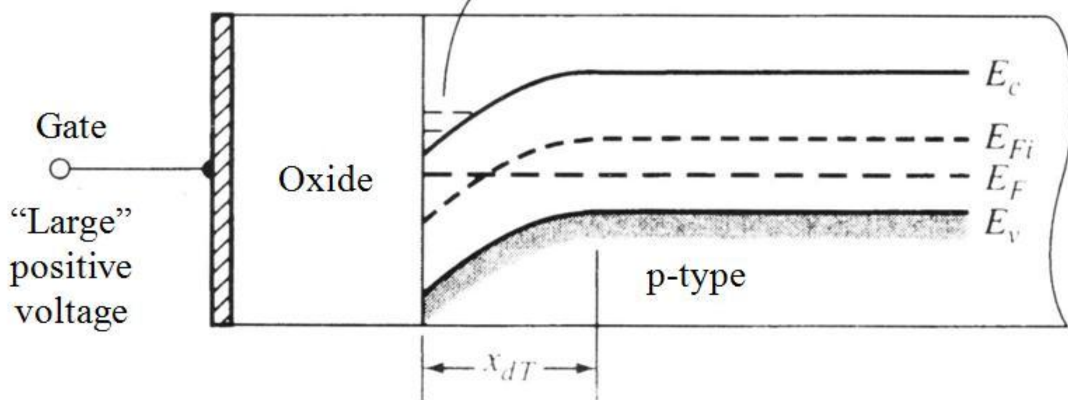

(c) Inversion

Fig. 2-2 Band diagram of a MOS-capacitor with a p-type substrate

2.1.2 MOS-Capacitor with N-type Substrate

Fig. 2-3 shows the band diagram of a MOS-capacitor with the n-type substrate. Under a positive gate voltage, the conduction band at the oxide/semiconductor interface bent downward and could be close to the Fermi level, and it means that there is electron-accumulation at the semiconductor surface as shown in Fig. 2-3(a).

Under a small negative gate voltage, valence band and intrinsic Fermi level bent upward and could be close to the Fermi level as shown in Fig. 2-3(b), and there is a depletion region occurs at the semiconductor surface. The depletion region expands with the increase of negative gate voltage.

As a much larger negative gate voltage is applied, the band bent even more as shown in Fig. 2-3(c). The intrinsic Fermi level at the interface is now higher than the Fermi level, so that it is p-type like at the oxide/semiconductor interface, which means the negative gate voltage starts to induce holes at the interface. In this case, the amount of minority carriers (holes) is greater than that of majority carriers (electrons) leading to the formation of an inversion layer.

By applying a high enough negative gate voltage, the carriers on the n-type substrate surface are inverted from n (electrons) to p (holes), and it is called the PMOS-capacitors.

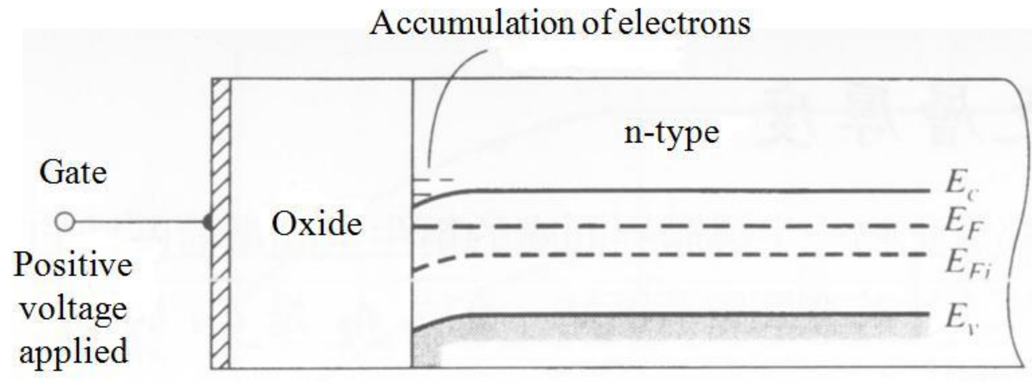

(a) Accumulation

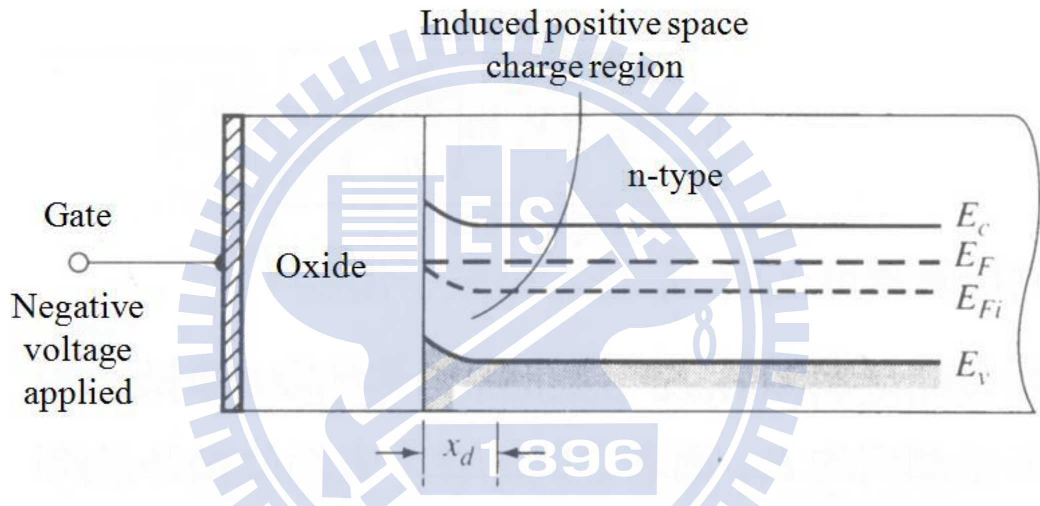

(b) Depletion

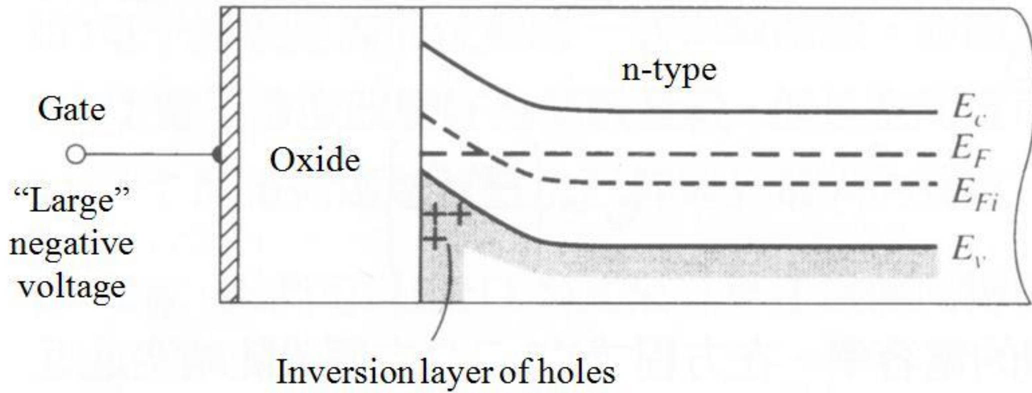

(c) Inversion

Fig. 2-3 Band diagram of a MOS-capacitor with a n-type substrate

2.1.3 MOS-Capacitor Characterization

The *C-V* measurements are widely used to quantitatively study MOS-capacitors. There are three important factors to evaluate the device performance, including flat-band voltage, hysteresis, and frequency dispersion. All of these factors are highly related with the quality of dielectric/semiconductor interface, as well as the interface trap density (D_{it}).

Flat-band Voltage

Flat-band voltage is used to determine the gate voltage at the condition of no bending in the semiconductor energy band diagram, which leads to no charge in the semiconductor, as shown in Fig. 2-4. And it is regarded as the ideal flat-band voltage. However, the real flat-band voltage would shift ΔV_{FB} due to there are trap charges exiting at the dielectric/semiconductor interface.

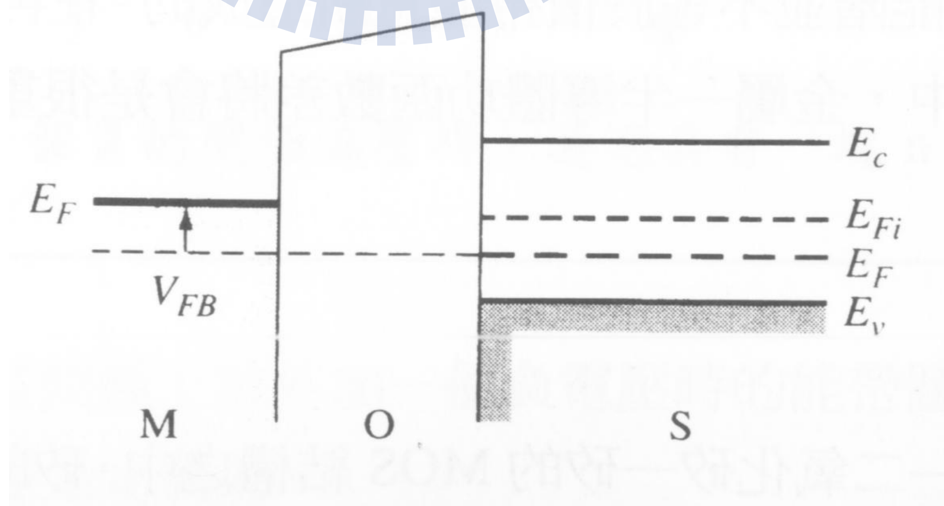

Fig. 2-4 Band diagram of flat-band condition of a MOS-capacitor [2-1]

Hysteresis

Hysteresis is measured a *C-V* curve under a certain frequency by sweeping the gate voltage forth and back. The amount of hysteresis is related with the amount of charges trapped by the defects in the gate dielectric, so that it can be used to determine the dielectric quality. The clockwise hysteresis implies the negative charges are trapped；On the other hand, the counterclockwise hysteresis implies the positive charges are trapped. The defects extracted from hysteresis are called as slow trapping states, and the interface traps are fast trapping states.

Frequency Dispersion

Frequency dispersion is the phenomenon of accumulation capacitance varying with different operated frequencies. The origin of frequency dispersion is related to the poor quality of dielectric/semiconductor interface, where there are a large amount of interface traps exiting. The interface traps are frequency dependent, and they would capture and emit charges leading to frequency dispersion of a *C-V* curve. Seriously, interface traps would cause Fermi level pinning degrading device performance.

2.2 Requirements for Gate Dielectrics

The number of transistors in a chip would be greatly increased following Moore's law [2-2, 2-3]. Based on the scaling rule proposed by Dr. R. Dennard, scaling down of MOSFETs brings not only integration of transistors but also improvement of device performance. The concept of scaling rule is illustrated in Fig. 2-5 and Table 2-1 [2-4].

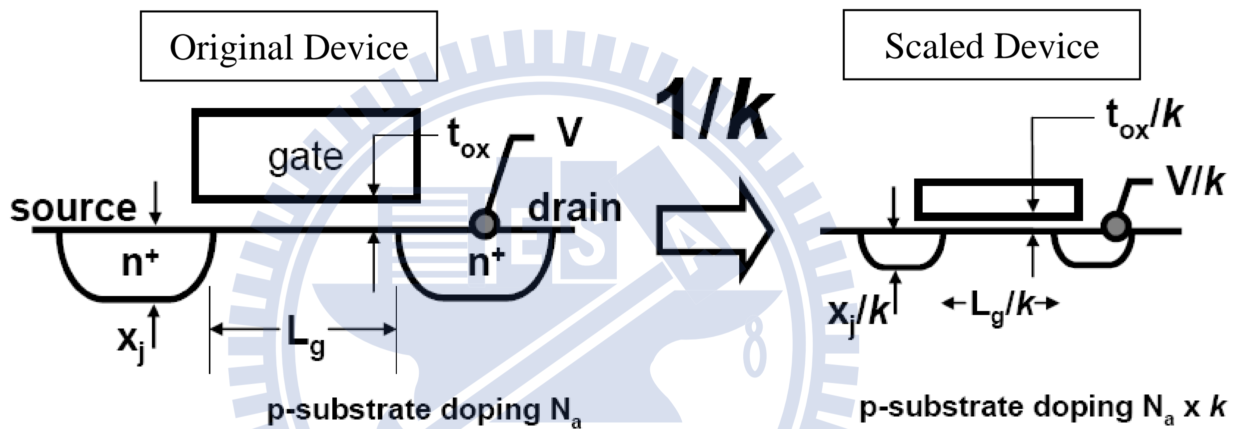

Fig. 2-5 Concept of scaling rule

Table 2-1 Scaling down of MOSFETs by a scaling factor of k

Quantity	Before Scaling	After Scaling (k>1)
Channel Length	L	L/k
Channel Width	W	W/k
Device Area	A	A/k^2
Gate Oxide Thickness	t_{ox}	t_{ox}/k
Gate Capacitance per Unit Area	C_{ox}	C_{ox}*k
Junction Depth	Xj	Xj/k
Power Supply Voltage	V_{DD}	V_{DD}/k
Threshold Voltage	Vth	Vth/k
Delay Time	t_d	t_d/k
Required Power	$V_{DD}I$	$V_{DD}I/k^2$
Doping Densities	N_A N_D	N_A*k N_D*k

However, ITRS roadmap predicts the limit of the size of transistors about 22 nm node, which probably leads to a serious gate leakage current due to an ultra-thin gate oxide layer. As shown in Fig. 2-6, the equivalent oxide thickness (EOT) lead to be 1nm after 2010, so it is hard to suppress the gate leakage current by using a sub-1nm SiO_2. Thus, semiconductor technology focused on the alternative gate dielectrics with high dielectric constant (κ) compared to SiO_2 [2-5]. In the last decade, high-κ gate dielectrics have shown necessary for scaling down the equivalent oxide thickness (EOT) with a physically thicker film and a low gate leakage current, as shown in Fig. 2-7. The relationship between physical thickness of SiO_2 and high-κ gate oxides extracted by the same capacitance value (C) is expressed as：

$$C = \frac{\varepsilon_{high\text{-}\kappa}}{t_{high\text{-}\kappa}} = \frac{\varepsilon_{SiO2}}{t_{EOT}} \qquad (2\text{-}1)$$

where $\varepsilon_{high\text{-}\kappa}$ is the dielectric constant of high-κ materials, $t_{high\text{-}\kappa}$ is the physical thickness of high-κ gate oxides, ε_{SiO2} is the dielectric constant of SiO_2 ($\kappa = 3.9$).

EOT (equivalent oxide thickness) is expressed as：

$$t_{EOT} = \frac{\varepsilon_{SiO2}}{\varepsilon_{high\text{-}\kappa}}\ t_{phy} \qquad (2\text{-}2)$$

where t_{phy} is the physical thickness of gate oxide materials.

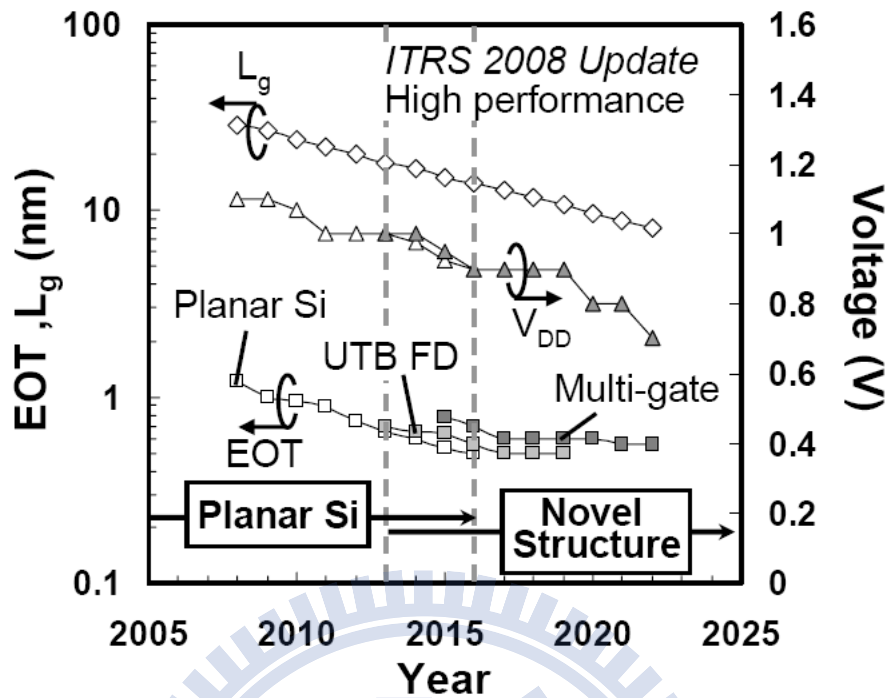

Fig. 2-6 Required physical gate length, equivalent oxide thickness (EOT) and supply voltage for the next 15 years reported on ITRS 2008 update

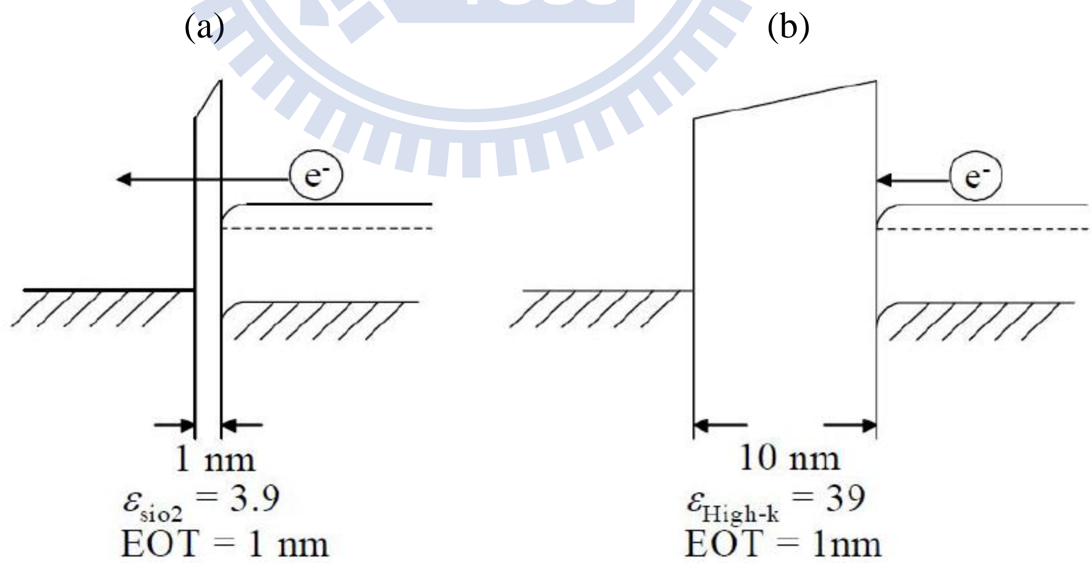

Fig. 2-7 Schematic illustration of gate leakage current under the different gate dielectrics of the MOS structure with (a) SiO_2 (b) High-κ

2.3 High-κ Gate Materials

The possible candidates of metal oxides to be used as gate dielectric materials are shown in the white squares of Table 2-2. Among these materials, Al_2O_3 is the most attractive material for the high-κ gate dielectric which has been widely experimented in MOS devices in the last decade [2-6~2-10]. Al_2O_3 shows the excellent dielectric properties, including a high dielectric constant (κ~9), a large energy band-gap (~9eV), a high breakdown electric field (5-30 MV/cm), high thermal and chemical stability, and its amorphous crystal structure can be used as the gate leakage tunneling barrier.

Table 2-2 Candidates for the metal, oxide of which has possibility to be used as high-κ gate insulator on periodic table

● = Not a solid at 1000 K
○ = Radioactive
① = Failed reaction 1: $Si + MO_x \rightarrow M + SiO_2$
② = Failed reaction 2: $Si + MO_x \rightarrow MSi_x + SiO_2$
⑥ = Failed reaction 6: $Si + MO_x \rightarrow M + MSi_xO_y$

● H																	● He
Li	Be											● B	● C	● N	● O	● F	● Ne
① Na	Mg											Al	Si	● P	● S	● Cl	● Ar
K	Ca	Sc	② Ti	① V	① Cr	① Mn	① Fe	① Co	① Ni	① Cu	① Zn	① Ga	① Ge	● As	● Se	● Br	● Kr
● Rh	Sr	Y	Zr	① Nb	① Mo	Tc	① Ru	① Rb	① Pd	● Ag	① Cd	① In	① Sn	① Sb	① Te	● I	● Xe
● Cs	⑥ Ba	R	Hf	① Ta	① W	① Re	① Os	① Ir	● Pt	● Au	● Hg	● Tl	① Pb	① Bi	○ Po	○ At	○ Rn
○ Fr	○ Ra	A	○ Rf	○ Ha	○ Sg	○ Ns	○ Hs	○ Mt									

R	La	Ce	Pr	Nd	○ Pm	Sm	Eu	Gd	Tb	Dy	Ho	Er	Tm	Yb	Lu
A	○ Ac	○ Th	○ Pa	○ U	○ Np	○ Pu	○ Am	○ Cm	○ Bk	○ Cf	○ Es	○ Fm	○ Md	○ No	○ Lr

In recent years, the group of Hf-based oxide materials has been gradually emphasized as shown in Fig. 2-8. Due to the eminent dielectric properties, such as the higher dielectric constant compared to Al_2O_3 (κ~20-25), a large energy band-gap (~6eV), low bulk trap densities and a large band offset (1.3-1.5eV). Hf-based oxides were adopted as the gate dielectric for the 45nm transistors in 2007 by Intel [2-11].

On the other hand, rare-earth oxides (REOs) are also regarded as the selection for the next generation of technology nodes. Among rare-earth oxides, La_2O_3 is considered one of the most attractive materials due to its promising properties such as a high dielectric constant (*κ*~27), a large band gap (~6eV) and conduction-band offset (2.3eV), a high breakdown electric field (>13MV/cm), and a low leakage current. Also, CeO_2 exhibits a wide dielectric constant range (*κ*~25-52) based on its crystal structure, but the smaller band gap and conduction-band offset can cause a larger leakage current [2-12].

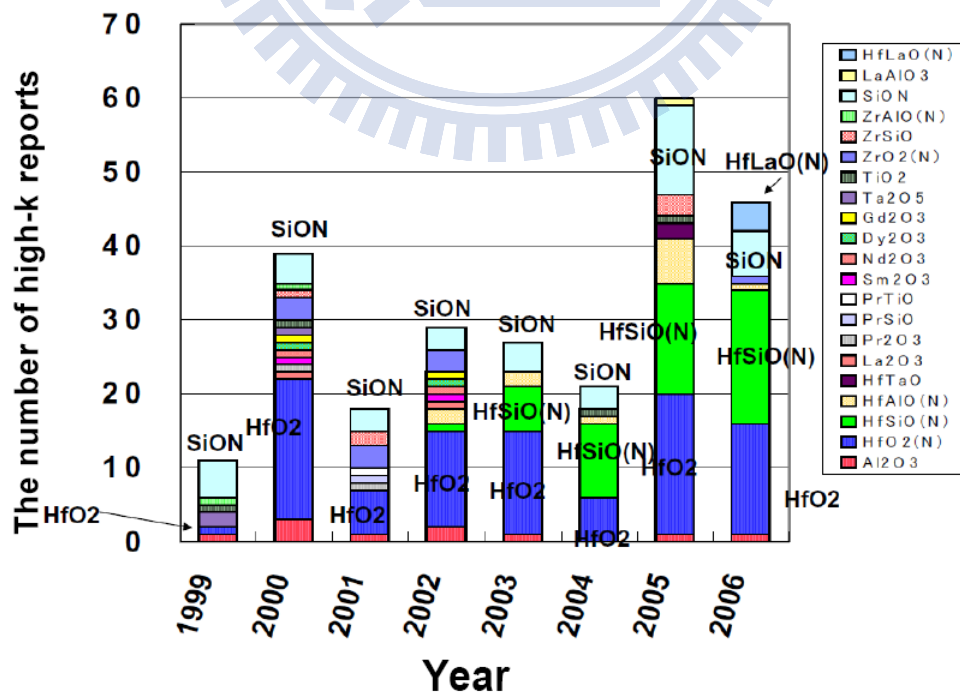

Fig. 2-8 Recent high-κ reports had been published in VLSI and IEDM symposium

2.4 III-V Compound Semiconductors as Channel Materials

Besides the gate oxide limitation, it is also difficult to continually improve the transistor performance as the device dimension decreases, which gives rise to some serious problems, such as short-channel effect, velocity saturation of channel carrier, large series resistance of source/drain layers, increase of source/drain leakage current [2-13]. Thus, conventional Si MOS-devices are confronted by the scaling limit for the gate length under 15~20nm.

According to the drain current equation of MOSFETs, $I_d = \frac{W}{L}\mu_{eff}\frac{\varepsilon_{ox}}{T_{ox}}(V_g\text{-}V_t)V_d$, it can be also the alternative method to improve device performance without scaling down by increasing effective carrier-mobility. In fact, enhancing carrier mobility has already been investigated by means of strained channel [2-14~2-16]. The most effective method is replacing Si with high carrier mobility materials as the channel layer, thus, high carrier-mobility materials attracted a lot of attention recently. Especially, III-V compound semiconductors have been extensively studied due to the much higher carrier mobility compared to Si as listed in Table 2-3. Therefore, performance improvement of MOS-devices with a high carrier-mobility channel is expected.

Table 2-3 Electron and hole mobility of various semiconductors

	Si	**Ge**	**GaAs**	**InP**	**$In_XGa_{1\text{-}X}As$**
electron mob. **μ_e (cm^2/Vs)**	**1350**	**3900**	**8500**	**5400**	**8000~30000**
hole mob. **μ_h (cm^2/Vs)**	**480**	**1900**	**400**	**200**	**400~600**

Chapter 3

Fabrication of III-V Metal-Oxide-Semiconductor Capacitors

3.1 Experimental Process Flow

Fig. 3-1 summaries the fabrication flow of $In_XGa_{1-X}As$ MOS-capacitors. The first step was wafer cleaning by using ACE and IPA to remove the contamination on the wafer surface. After that, surface treatment was performed before the gate dielectric deposition. For the surface treatment, dilute HF solution was first used to eliminate the native oxide on the wafer surface, and then treated with $(NH_4)S_X$ solution for 20～30 minutes at room temperature. A passivation layer which was favorable for the gate dielectrics deposition would be formed on the wafer surface. After the surface treatment, high-κ gate materials were deposited by electron-beam deposition in an ultra high vacuum chamber at a pressure of 10^{-8} Pa, and then annealed by the RTA system to improve the quality of oxide/semiconductor interface. Finally, tungsten (W) was chosen as the gate metal and the backside ohmic metal used was gold (Au), which were deposited by the E-gun evaporation system.

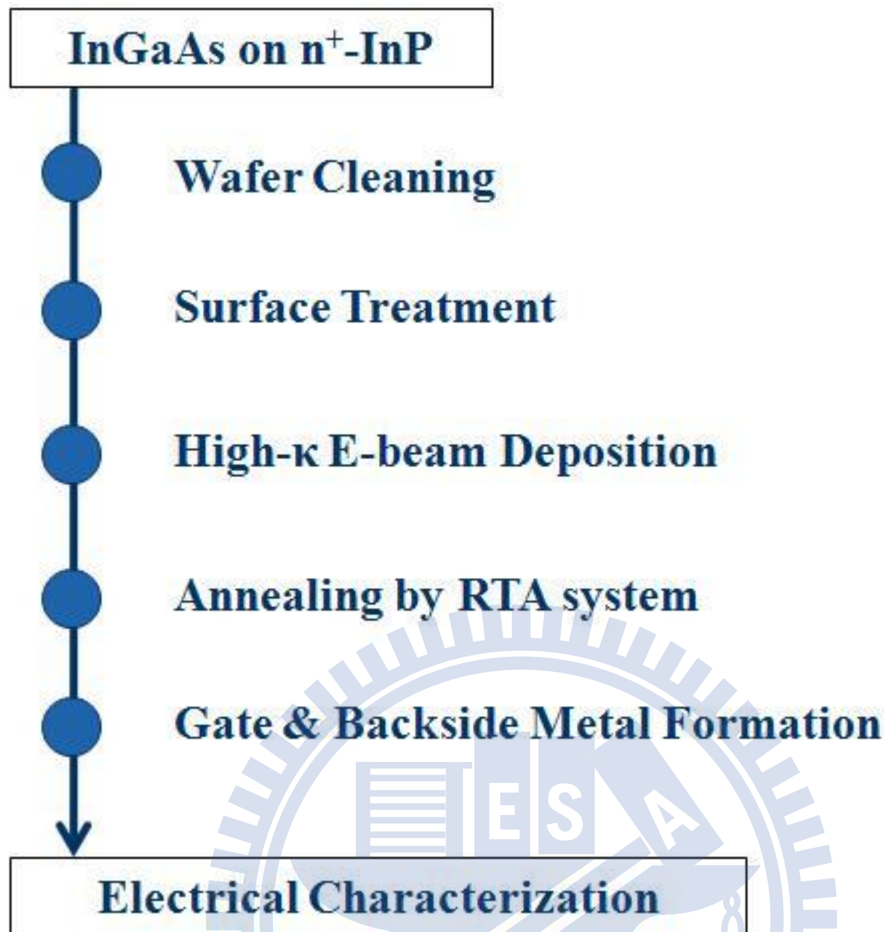

Fig. 3-1 Fabrication process flow of III-V MOS-capacitors

3.2 Electron Beam Epitaxy (MBE) [3-1]

The high-κ gate dielectrics were deposited under an ultra-high vacuum by the MBE system as shown in Fig. 3-2. The background pressure in the chamber was in the 10^{-8} Pa range and was in the 10^{-7} Pa range during the deposition process. In the chamber, the sintered high-κ target was the evaporation source and was heated up by irradiating with electron beam accelerated to 5keV. Then, an ultra-thin high-κ film was deposited on the substrate. Physical thickness of the film was monitored by a film thickness monitor using the crystal oscillator. The temperature of the substrate was controlled by a substrate heater and was measured by a thermocouple.

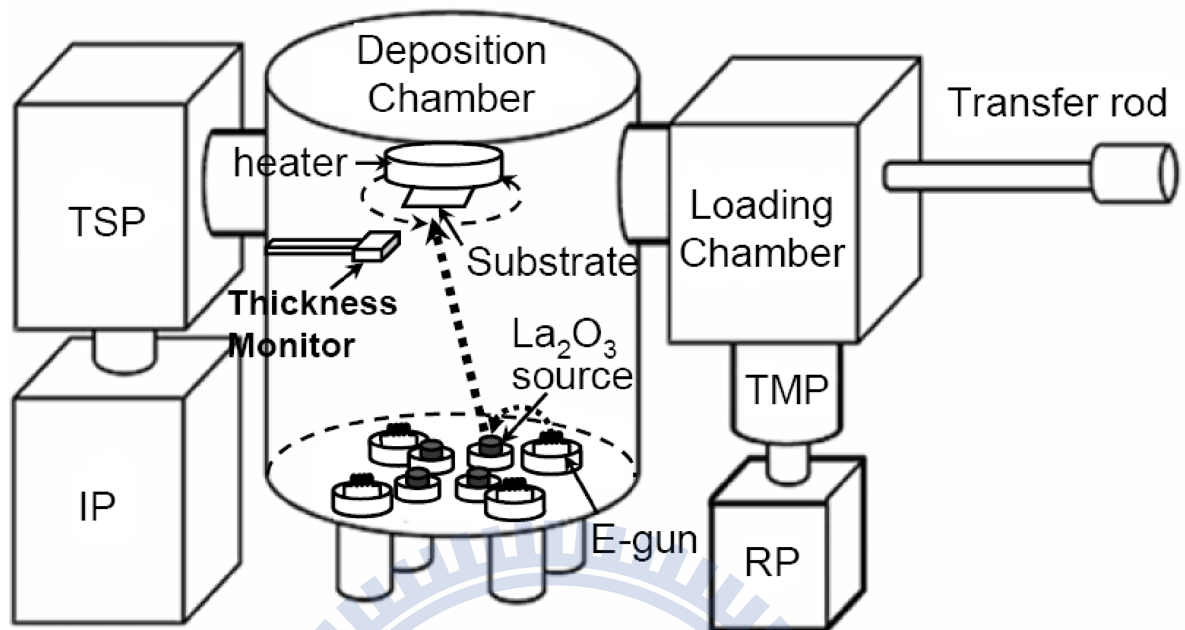

Fig. 3-2 Schematic of the MBE chamber for the deposition of high-κ gate materials

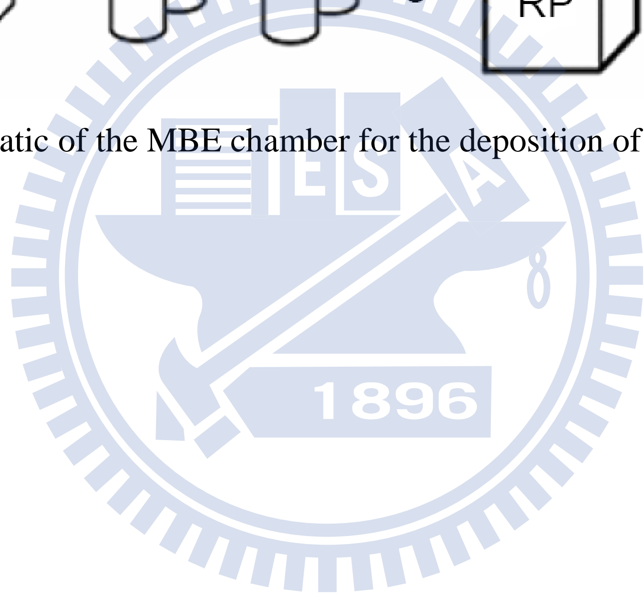

Chapter 4

Fundamentals of Electrical Characteristics for III-V MOS-Capacitors

4.1 Capacitance-Voltage (*C-V*) Characteristics [4-1]

C-V characteristic measurements were carried out under various frequencies by precision LCR meter. The energy band diagram of a MOS-capacitor on a p-type substrate is shown in Fig. 4-1. The intrinsic energy level E_i or potential Φ in the neutral part of device is taken as the zero reference. The surface potential, Φ_S, is measured from the reference level. The capacitance is defined as：

$$C = \frac{dQ}{dV} \tag{4-1}$$

where Q_G and V_G are the gate charge and the gate voltage, respectively. It is the change of charge due to a change of voltage and is most commonly given in units of farad/units area.

During capacitance measurements, a small-signal ac voltage is applied to the device. The resulting charge variation gives rise to the capacitance. Looking at a MOS capacitor from the gate, $C = dQ_G / dV_G$, where Q_G and V_G are the gate charge and the gate voltage. Since the total charge in the device must be zero, assuming no oxide charge, $Q_G = -(Q_S + Q_{it})$, where Q_S is the semiconductor charge, and Q_{it} is the interface charge. The gate voltage is partially dropped across the oxide and partially across the semiconductor. This gives $V_G = V_{FB} + V_{OX} + \Phi_S$, where V_{FB} is the flatband voltage, V_{OX} is the oxide voltage, and Φ_S is the surface potential, allowing Eq. (4-1) to be rewritten as：

$$C = \frac{dQ_S + dQ_{it}}{dV_{OX} + d\Phi_S} \tag{4-2}$$

The semiconductor charge density Q_S consists of hole charge density Q_p, space-charge region bulk charge density Q_b, and electron charge density Q_n. With $Q_S = Q_p + Q_b + Q_n$, Eq. (4-2) leads to：

$$C = -\frac{1}{\dfrac{dV_{OX}}{dQ_S + dQ_{it}} + \dfrac{d\Phi_S}{dQ_p + dQ_b + dQ_n + dQ_{it}}} \tag{4-3}$$

Based on the general capacitance definition of Eq. (4-1), Eq. (4-3) is expressed as：

$$C = -\frac{1}{\dfrac{1}{C_{ox}} + \dfrac{1}{C_p + C_b + C_n + C_{it}}} = \frac{C_{ox}\,(C_p + C_b + C_n + C_{it})}{C_{ox} + C_p + C_b + C_n + C_{it}} \tag{4-4}$$

The positive accumulation Q_p dominates under negative gate voltages for p-substrate devices. For positive V_G, the semiconductor charges are negative. The minus sign in Eq. (4-3) cancels in either case. Eq. (4-4) is represented by the equivalent circuit in Fig. 4-2(a). Under negative gate voltages, the surface is heavily accumulated and Q_p dominates. C_p is very high approaching a short circuit. Hence, the four capacitances are shorted as shown by the heavy line in Fig. 4-2(b) and the overall capacitance is C_{ox}. For small positive gate voltages, the surface is depleted and the space-charge region charge density, $Q_b = qN_AW$, dominates. Trapped interface charge capacitance also contributes. The total capacitance is the combination of C_{ox} in series with C_b in parallel with C_{it} as shown in Fig. 4-2(c). In weak inversion C_n begins to appear. For strong inversion, C_n dominates because Q_n is very high. If Q_n is able to follow the applied ac voltage, the low-frequency equivalent circuit (Fig. 4-2(d)) becomes

the oxide capacitance again. When the inversion charge is unable to follow the ac voltage, the circuit in Fig. 4-2(e) applies in inversion, with C_b = K_s ε_o / W_{inv} with W_{inv} the inversion space-charge region width.

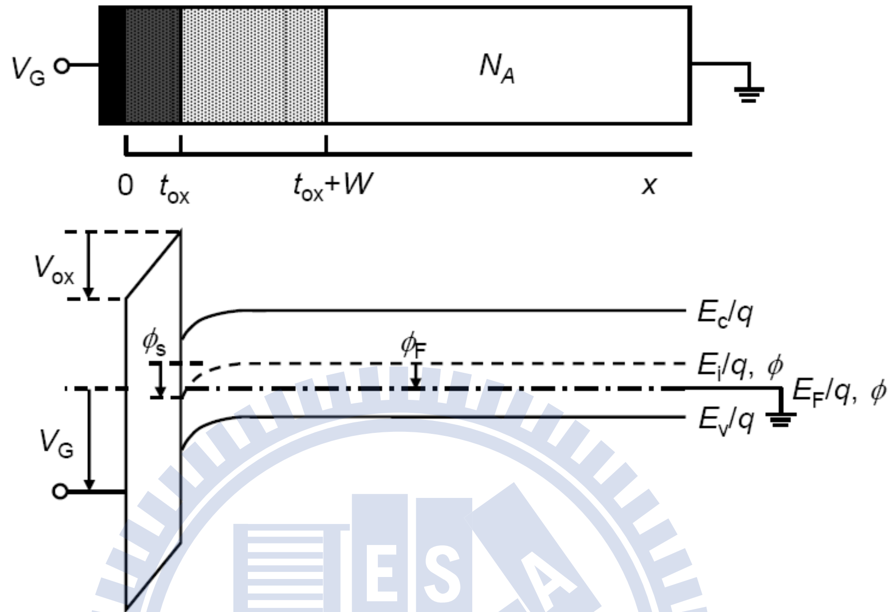

Fig. 4-1 Cross-section and band diagram of a MOS-capacitor

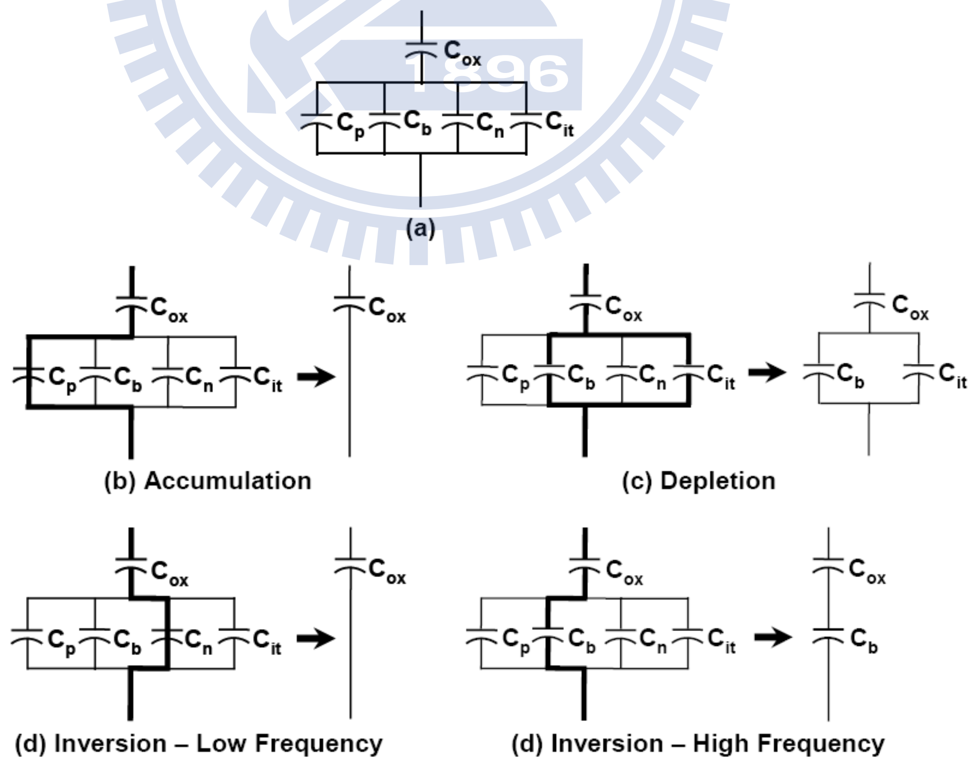

Fig. 4-2 Capacitances of MOS-capacitors under the different bias conditions

4.2 Leakage Current Density-Voltage (*J-V*) Characteristics

To reduce the power consumption, it is essential to suppress the gate leakage current of MOS devices as small as possible. *J-V* measurement is used to estimate the leakage current density. The measurement started at 0 V and sweep towards accumulation region until breakdown occurs.

4.3 Interface Trap Density (D_{it}) by Conductance Method

The conductance method, proposed by Nicoliian and Goetzberger in 1967, is one of the most sensitive methods to determine D_{it} [4-2]. The technique is based on measuring the equivalent parallel conductance G_p of a MOS capacitor as a function of bias voltage and frequency. The conductance, representing the loss mechanism due to interface trap capture and emission of carriers, is a measure of the interface trap density.

The simplified equivalent circuit of a MOS-capacitor appropriate for the conductance method is shown in Fig. 4-3(a). It consists of the oxide capacitance C_{ox}, the semiconductor capacitance C_s, and the interface trap capacitance C_{it}. The capture-emission of carriers by D_{it} is a lossy process, represented by the resistance R_{it}. It is convenient to replace the circuit of Fig. 4-3(a) by that in Fig. 4-3(b), where C_p and G_p are given by：

$$C_p = C_s + \frac{C_{it}}{1 + (\omega\tau_{it})^2} \tag{4-5}$$

$$\frac{G_p}{\omega} = \frac{q\omega\tau_{it} D_{it}}{1 + (\omega\tau_{it})^2} \tag{4-6}$$

where $C_{it} = q^2 D_{it}$, $\omega = 2\pi f$ (f = measurement frequency) and $\tau_{it} = R_{it}C_{it}$, the interface trap time constant, given by $\tau_{it} = [\upsilon_{th}\sigma_p N_A \exp(-q\varphi_s / kT)]^{-1}$. Dividing G_p by ω makes Eq. (4-6) symmetrical in $\omega\tau_{it}$. Equations (4-5) and (4-6) are for interface traps with a single energy level in the band gap. Interface traps at the insulator/semiconductor interface, however, are continuously distributed in energy throughout the semiconductor band gap. Capture and emission occurs primarily by traps located within a few kT/q above and below the Fermi level, leading to a time constant dispersion and giving the normalized conductance as

$$\frac{G_p}{\omega} = \frac{qD_{it}}{2\omega\tau_{it}} \ln[1 + (\omega\tau_{it})^2] \qquad (4\text{-}7)$$

The conductance is measured as a function of frequency and plotted as G_p/ω versus ω. G_p/ω has a maximum at $\omega = 1/\tau_{it}$ and at that maximum $D_{it} = 2G_p/q\omega$. For Eq. (4-7), one can find $\omega \sim 2/\tau_{it}$ and $D_{it} = 2.5G_p/q\omega$ at the maximum. Hence, one can determine D_{it} from the maximum G_p/ω and determine τ_{it} from ω at the peak conductance location on the ω-axis.

An approximate expression of the interface trap density in terms if the measured maximum conductance is

$$D_{it} = \frac{2.5}{q}\left(\frac{G_p}{\omega}\right)_{\max} \qquad (4\text{-}8)$$

Capacitance meters generally assumed the device consist of the parallel C_m-G_m combination in Fig. 4-3(c). A circuit comparison of Fig. 4-3(b) to 4-3(c) gives G_p/ω in terms of the measured capacitance C_m, the oxide capacitance, and the measured conductance G_m as

$$\frac{G_p}{\omega} = \frac{\omega G_m C_{ox}^2}{G_m^2 + \omega^2 (C_{ox} - C_m)^2} \qquad (4\text{-}9)$$

assuming negligible series resistance. The conductance measurement must be

carried out over wide frequency range. The portion of the band gap probed by conductance measurements is typically from flat-band to weak inversion. The measured frequency should be accurately determined and the signal amplitude should be kept at around 50mV or less to prevent harmonics of the signal frequency giving rise to spurious conductance.

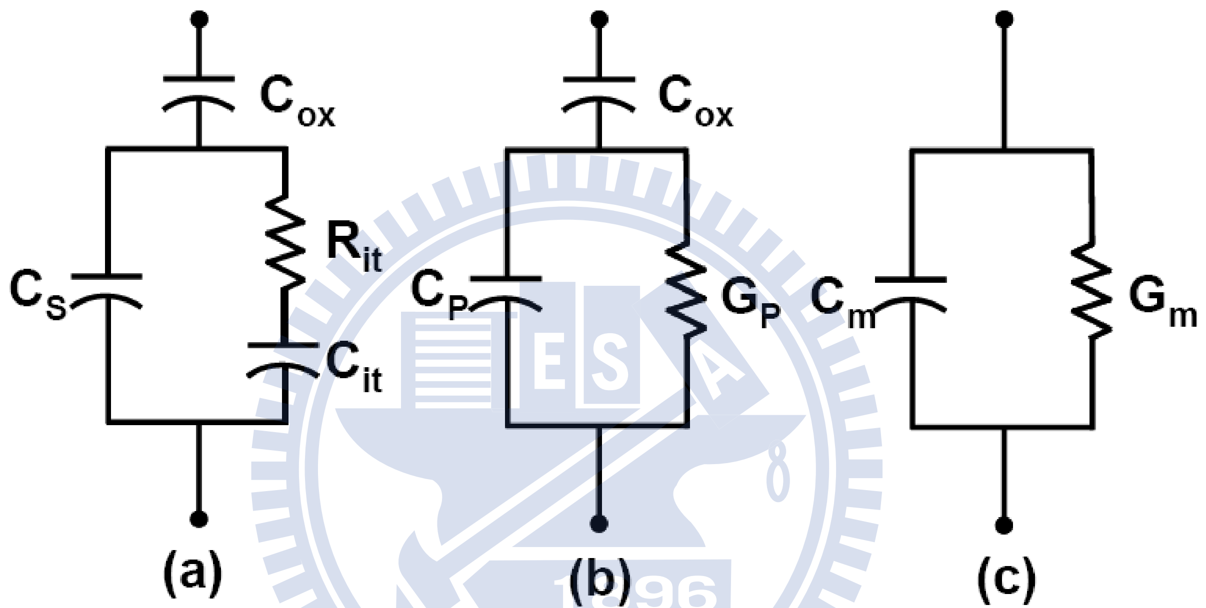

Fig. 4-3 Equivalent circuit for conductance measurement (a) MOS-C with interface trap time constant $\tau_{it} = R_{it}C_{it}$, (b) simplified circuit of (a), (c) measured circuit

Chapter 5

Experimental Results and Discussion

5.1 Study on Electrical Characteristics of HfO_2/n-InAs Metal-Oxide-Semiconductor Capacitors with Different Post Deposition Annealing Temperatures

5.1.1 Introduction

For future scaling of complimentary metal-oxide-semiconductor (CMOS) technology in accordance with Moore's Law, it will require novel solutions such as high-κ dielectrics, metal gates, and high carrier-mobility channels. Recently, III-V metal-oxide-semiconductor field-effect transistors (III-V MOSFETs) have been extensively investigated for future high speed and low power logic applications by using the use of III-V high mobility channels and high-κ gate dielectrics [5-1]. Among III-V materials, InAs has much higher carrier-mobility exhibiting the superior transport property for device performance [5-2~5-4]. Therefore, InAs is an excellent candidate as the channel material for the next generation of CMOS logic circuits. In addition, a high-κ gate dielectric has been used to improve MOS-device performance, including reducing the gate leakage current with a physically thicker gate dielectric thickness, and enhancement of logic characteristics [5-5]. Among high-κ dielectrics, Hf-based dielectrics, especially HfO_2, are considered as ideal high-κ materials for the next CMOS generation due to their high dielectric constant (κ~20-25) and high energy

band-gap (~6eV).

Before realization of III-V CMOS utilizing InAs as the channel material, it is essential to obtain the high quality of dielectric/InAs interface with the minimal hysteresis and a low interface trap density (D_{it}). Thus, the HfO_2/n-InAs MOS-capacitors were fabricated and the device performance was evaluated under the different post deposition annealing (PDA) temperatures in this study. Moreover, the device performance of HfO_2/n-InAs MOS-capacitor was also compared with that of Al_2O_3/n-InAs MOS-capacitor.

5.1.2 Experiment

The structure of the n-InAs MOS-capacitor in this study is as shown in Fig. 5-1-1, and the wafer structure was grown by molecular beam epitaxy (MBE) on a 3-in n^+-InP substrate. The structure layers, from bottom to top, are composed of a 10-nm-thick n-$In_{0.53}Ga_{0.47}As$ (Si：$5x10^{17}cm^{-3}$), a 3-nm-thick n-$In_{0.70}Ga_{0.30}As$ (Si：$5x10^{17}cm^{-3}$), and a 5-nm-thick n-InAs (Si：$5x10^{17}cm^{-3}$).

The wafers were first cleaned in a dilute HF (50%) solution for 3 minutes, and then followed by surface treatment in a $(NH_4)_2S_X$ solution for 30 minutes at room temperature. The cleaned wafers were deposited an HfO_2 layer of 15nm at 300°C by the MBE system. After the gate oxide deposition, the post deposition annealing (PDA) process was performed with the different temperature conditions for 5 minutes, ranging from 400°C to 550^oC. After the PDA process, tungsten (W) metal (contact size: 50μm in diameter) was deposited as the gate metal by the lift-off process and gold (Au) metal was deposited by the sputtering process as the backside ohmic contact.

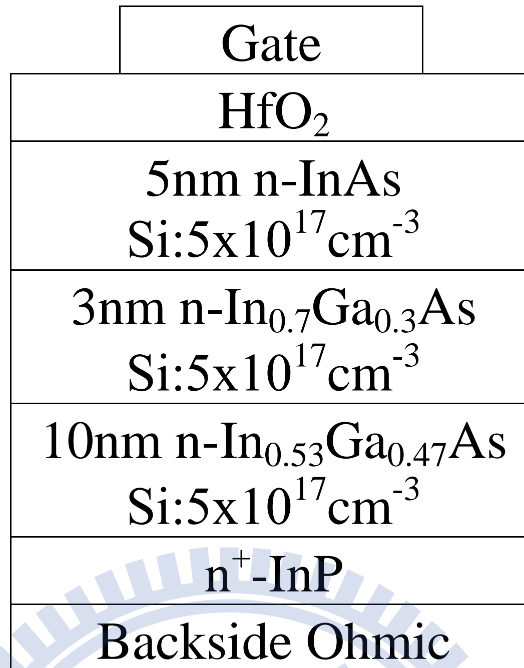

Fig. 5-1-1 Structure of the HfO_2/n-InAs MOS-capacitor

5.1.3 Results and Discussion

Transmission Electron Microscopy (TEM) Analysis

The interface of HfO_2/n-InAs MOS-capacitor was observed by the cross-sectional transmission electron microscopy (TEM) analysis as shown in Fig. 5-1-2(a). Compared to the HfO_2/n-$In_{0.53}Ga_{0.47}As$ MOS-capacitor (Fig. 5-1-2(b)) with the similar process conditions, there was less interfacial oxide formed at the HfO_2/n-InAs interface. The interfacial oxide layer at the HfO_2/n-$In_{0.53}Ga_{0.47}As$ interface was identified as Ga-oxide [5-6], which was absent at the interface of HfO_2/n-InAs MOS-capacitor as observed in Fig. 5-1-2(a).

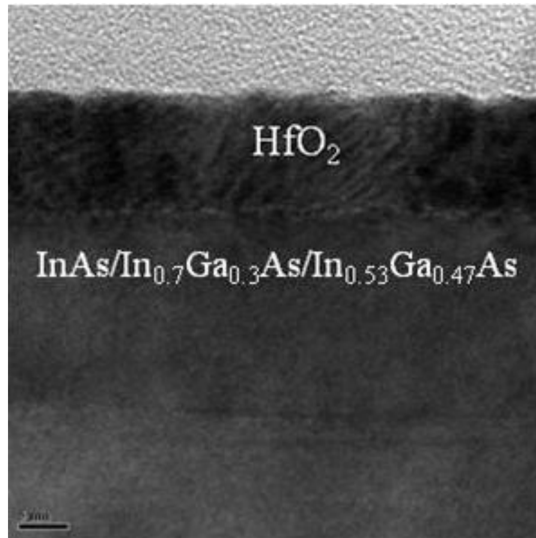

(a) HfO_2/InAs

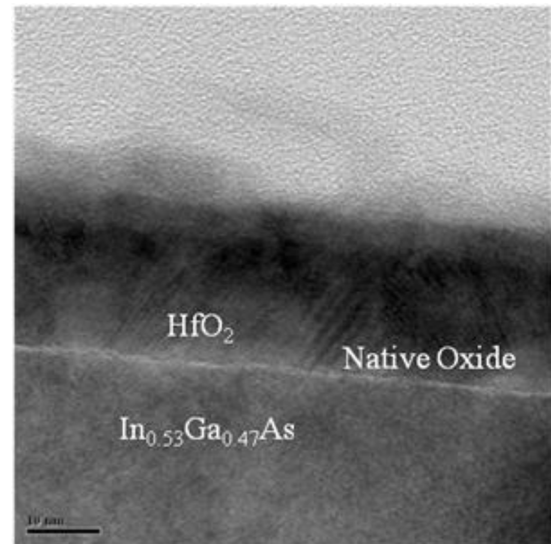

(b) $HfO_2/In_{0.53}Ga_{0.47}As$

Fig. 5-1-2 TEM images of interface (a) HfO_2/InAs, (b) $HfO_2/In_{0.53}Ga_{0.47}As$

C-V Characteristics

The *C-V* characteristics of HfO_2/n-InAs MOS-capacitors with the different PDA temperatures of 400°C, 450°C, 500°C and 550°C were shown in Fig. 5-1-3. The device annealed at 400°C had the highest capacitance value at the accumulation region among the annealing temperatures in this study and the capacitance value was reduced with the increase of PDA temperature. Furthermore, there was no clear saturation observed at the inversion region for the capacitor annealed at 400°C. The phenomenon may be due to a small amount of native oxide existed at the oxide/semiconductor interface. However, as the PDA temperature was increased to 450°C, the native oxide at the interface was reduced, leading to the obvious saturation at the inversion region.

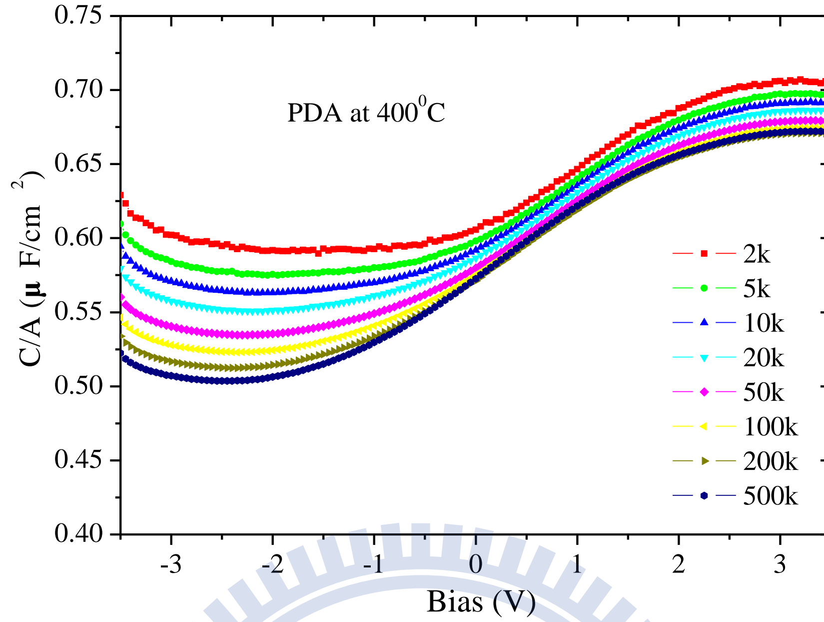

(a) 400°C

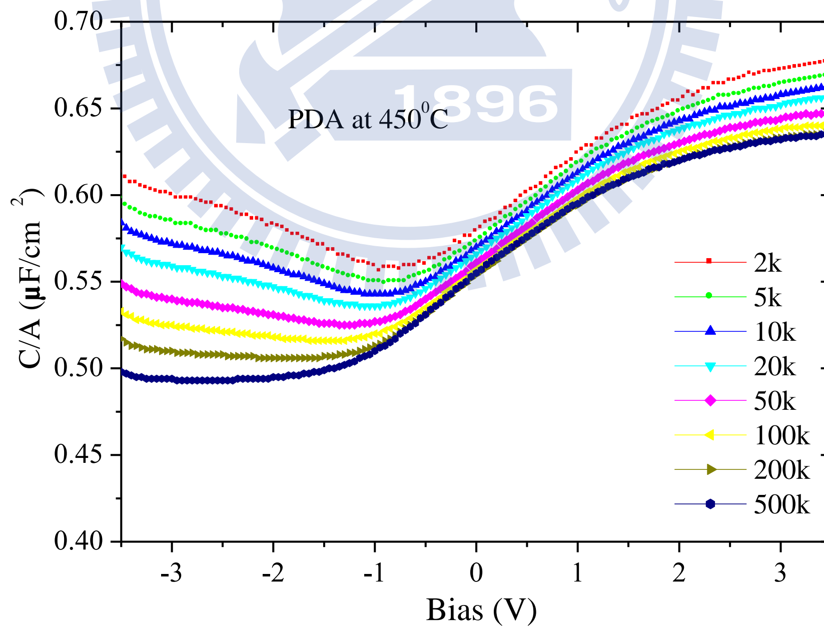

(b) 450°C

Fig. 5-1-3 *C-V* characteristics of the HfO_2/n-InAs MOS-capacitors after PDA at (a) 400°C (b) 450°C

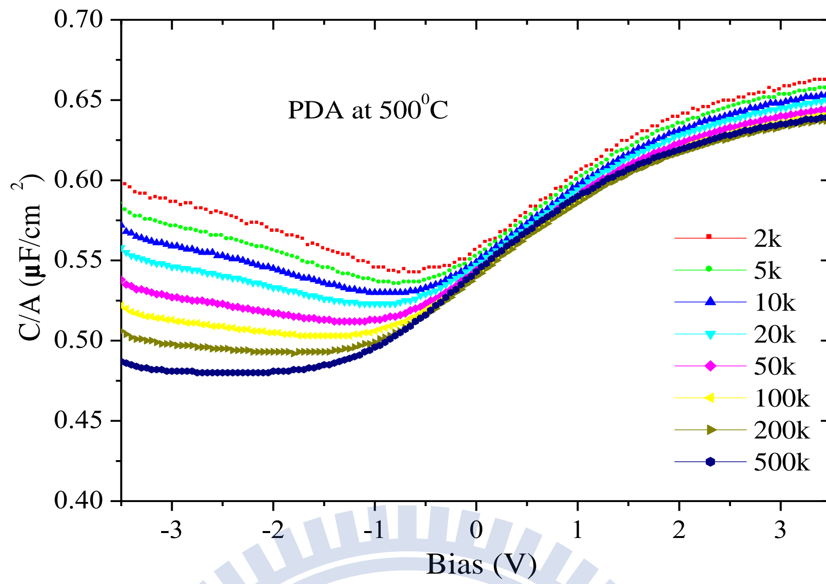

(c) 500°C

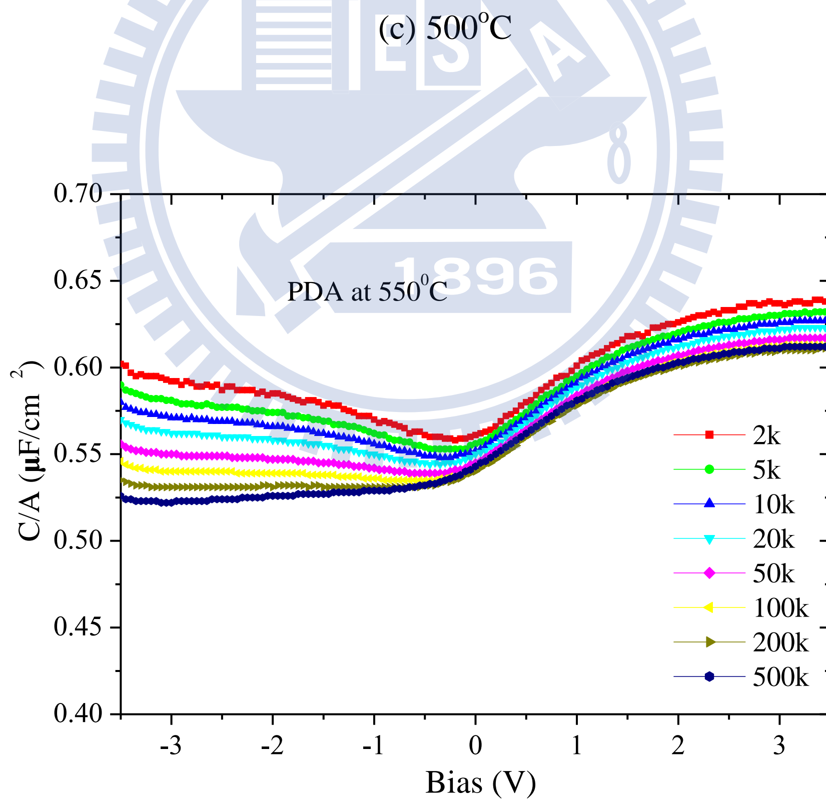

(d) 550°C

Fig. 5-1-3 *C-V* characteristics of the HfO_2/n-InAs MOS-capacitors after PDA at (c) 500°C (d) 550°C

The hysteresis behaviors of HfO_2/n-InAs MOS-capacitors at 100 kHz at the different annealing temperatures were investigated by using the bidirectional *C-V* sweeps as shown in Fig. 5-1-4. The behavior of hysteresis occurrence depends on the quality of the high-κ dielectric, it can be seen that the hysteresis voltage decreased with the increase of PDA temperature, which implied the quality of HfO_2 film was improved, especially at the PDA temperature of 500°C (ΔV=-37mV). However, as the PDA temperature approached 550°C, the hysteresis became worse (ΔV = -288 mV) due to a small amount of indium (In) diffused into HfO_2.

The flat-band voltage at 100 kHz shifted to a more negative value with the increase of PDA temperature from 400°C to 500°C, 2.15 V (400°C), 1.32 V (450°C), 1.11 V (500°C), which implied that the oxide charges were reduced under a higher PDA temperature. Also, the flat-band voltage shifted to a more positive value of 2.14 V at the PDA temperature of 550°C due to indium (In) diffusion. Furthermore, the capacitance value at the flat-band condition decreased with increasing annealing temperature.

The interface trap densities (D_{it}) of HfO_2/n-InAs MOS-capacitors at the different PDA temperatures were estimated by the conductance method. It showed that the device at the PDA temperature of 500°C had the lowest D_{it} with the value of $2.7\text{x}10^{12}$ cm$^{-2}\cdot$eV^{-1} among all the PDA temperatures studied. The leakage current for the 15nm HfO_2/n-InAs MOS-capacitor after 500°C annealing was less than 1×10^{-5}A/cm^{2} when the bias voltage was between -3.5 V to 3.5 V. All of the *C-V* characteristics mentioned above were listed in Table 5-1-1.

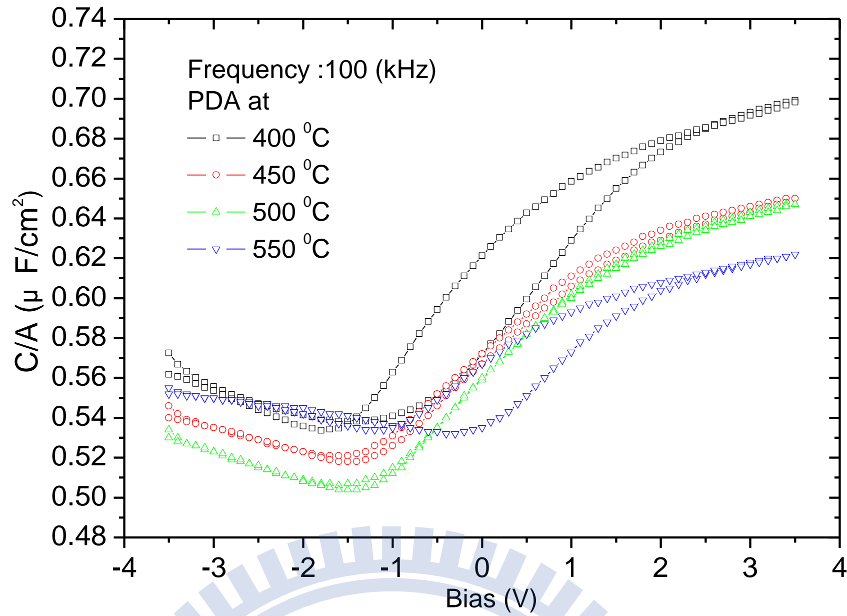

Fig. 5-1-4 Bidirectional *C-V* sweeps of the HfO_2/n-InAs MOS-capacitors at the different PDA temperatures

Table 5-1-1 Comparison of electrical characteristics of the HfO_2/n-InAs MOS-capacitors at the different PDA temperatures

PDA temp. (°C)	400	450	500	550
Flat-band voltage (V) @100kHz	2.178	1.319	1.113	2.138
C_{FB} (μF/cm^2)	0.677	0.621	0.606	0.606
Hysteresis (mV)	0.278	-0.189	-0.037	0.288
D_{it} (cm^{-2}e·V^{-1})	1.02x10^{13}	4.37x10^{12}	2.71x10^{12}	5.33x10^{12}

XPS Analysis

Fig. 5-1-5 showed the *XPS* spectra of HfO_2/n-InAs MOS-capacitors at the different PDA temperatures from 400°C to 550°C. There were three values of $In3d_{5/2}$, InO_X, In_2O_3 and InAs, and two values of As3d, As_2O_3 and InAs, observed. The native oxide of InAs, which is mainly composed of As_2O_3, is known to produce a relative poor interface.

According to the *XPS* results, it was observed that the amount of InO_X and As_2O_3 decreased when the PDA temperature was increased from 400°C to 450°C. As the PDA temperature approached 500°C, there was no clear As_2O_3 peak, and the device had the best hysteresis value of ~ 37mV as shown in Fig. 5-1-4. However, when PDA temperature was increased up to 550°C, a small amount of indium (In) diffused into HfO_2 and both In_2O_3 and InO_X amount increased as observed from the *XPS* results. And it was the reason that the electrical characteristics of HfO_2/n-InAs MOS-capacitor degraded at a PDA temperature over 500°C.

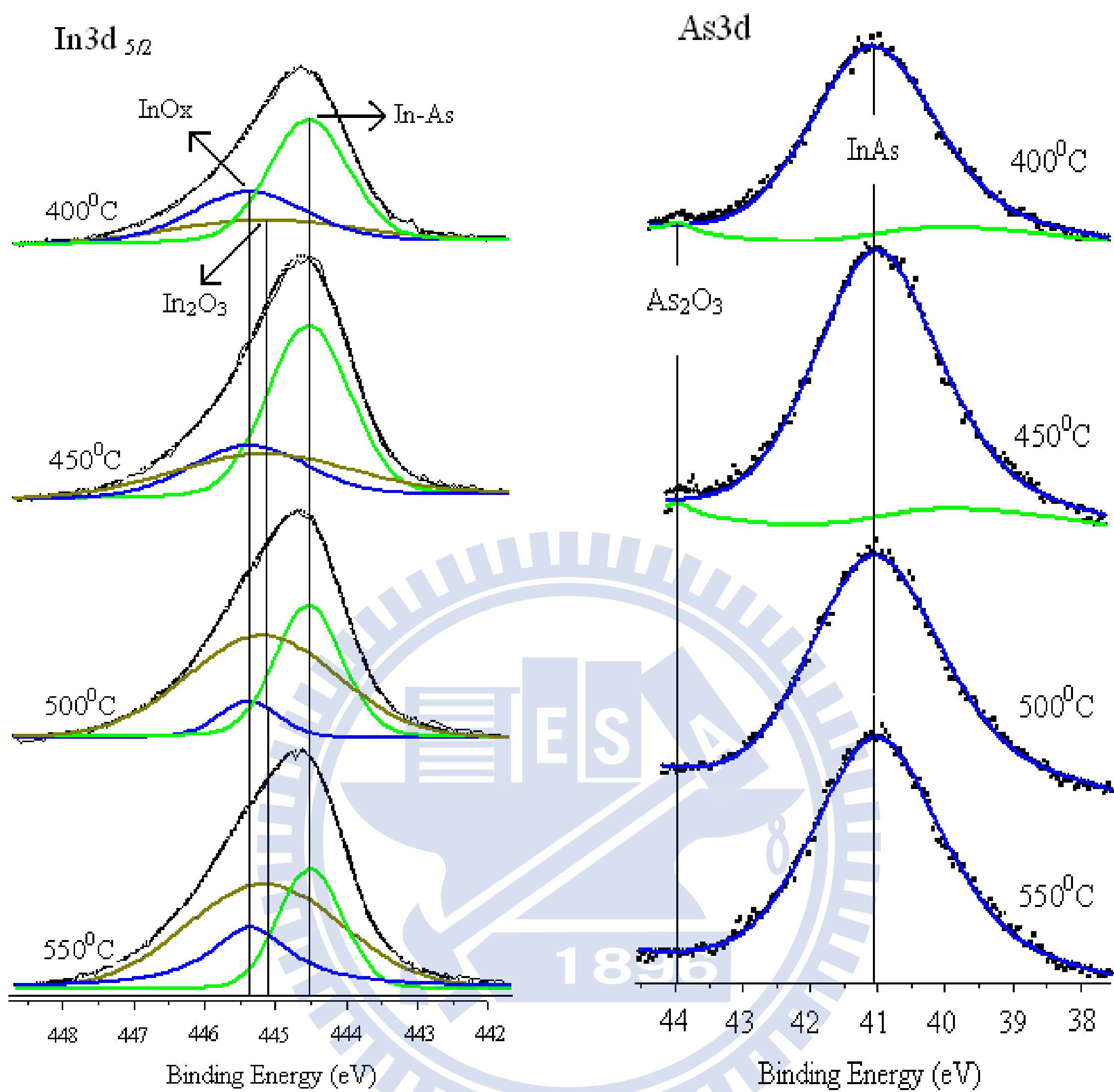

Fig. 5-1-5 *XPS* spectra of the HfO_2/n-InAs MOS-capacitors at the different PDA temperatures

Compared to Al_2O_3/n-InAs MOS-Capacitor

Al_2O_3 is the most mature high-κ material for III-V MOS-devices and have been investigated as the gate dielectric in recent years. Also, the study of Al_2O_3/n-InAs MOS-capacitors was already done by Dr. Yun-Chi, Wu before in our group [5-7]. The fabrication process of Al_2O_3/n-InAs MOS-capacitors was also the same as described in this thesis.

The *C-V* characteristic of Al_2O_3/n-InAs MOS-capacitor is shown in Fig. 5-1-6. Compared with the *C-V* characteristic of HfO_2 one at the same operated frequency (*f*：100 kHz), the MOS-capacitor with HfO_2 exhibited the capacitance value of 0.64 (pF/cm^2) at the accumulation condition which is higher than that of 0.54 (pF/cm^2) of Al_2O_3 MOS-capacitor. Furthermore, the HfO_2/n-InAs MOS-capacitor had the smaller equivalent oxide thickness (EOT). Table 5-1-2 lists the comparison of Al_2O_3 and HfO_2 n-InAs MOS-capacitors.

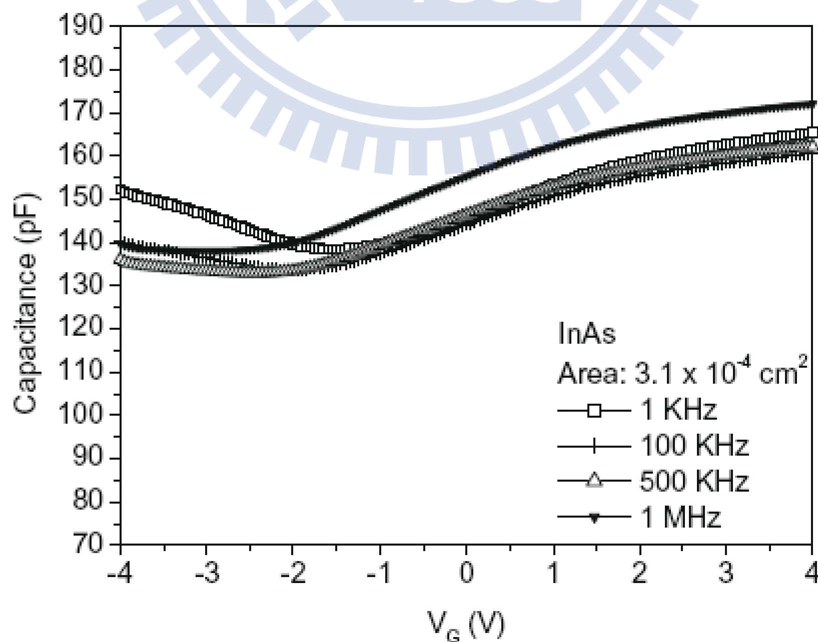

Fig. 5-1-6 *C-V* characteristics of the Al_2O_3/n-InAs MOS-capacitor

Table 5-1-2 Comparison of the Al_2O_3 and HfO_2/n-InAs MOS-capacitors

	κ	E_g (eV)	C_{Acc} (pF/cm^2) @100kHz	D_{it} (cm^{-2}e·V^{-1})	EOT (nm)
Al_2O_3	9	9	0.54	9 x10^{11}	6.768
HfO_2	20-25	6	0.64	2.71x10^{12}	5.393

5.1.4 Conclusion

The electrical characteristics of HfO_2/n-InAs metal-oxide-semiconductor capacitors with the different post deposition annealing (PDA) temperatures were demonstrated. By the use of InAs as the channel layer, it could avoid the undesired Ga-oxide formation at the dielectric/semiconductor interface compared to the $In_{0.53}Ga_{0.47}As$ channel device. Moreover, the quality of HfO_2/ InAs interface was improved with the increase of PDA temperature. The MOS-capacitor after 500°C PDA annealing demonstrated the lowest interface trap density (D_{it}) value due to the reduction of native oxide (As_2O_3), which was verified by the *XPS* results. Also, the *C-V* characteristics of device with 500°C annealing exhibited the best performance such as a lowest hysteresis value, the flat-band voltage shifted to a more negative value, and the smaller frequency dispersion at the accumulation region. However, as the annealing temperature approached 550°C, a small number of indium (In) atoms diffused into the HfO_2 layer with the increase of InO_X and In_2O_3 formation so that the device performance was degraded. On the other hand, the HfO_2/n-InAs MOS-capacitor had the higher capacitance value and the smaller equivalent oxide thickness (EOT) compared to the device with the Al_2O_3 gate dielectric.

5.2 Performance Improvement of Bilayer High-κ Gate Dielectrics for $In_XGa_{1-X}As$ Metal-Oxide-Semiconductor Capacitors

5.2.1 Introduction

For the CMOS technologies perhaps approach the limit of development by the forecast of Moor's Law. To extent CMOS technique to 22 nm node and beyond, it requires alternate materials and structures for future devices for logic and low power applications. Recently, researchers have been paying attention to III-V high mobility channel materials, especially high indium (In) content $In_XGa_{1-X}As$, that potentially provides high carrier transport and drive current with small effective mass [5-8~5-9]. Thus, III-V compound semiconductors are considered as the most attractive alternate channel materials to replace silicon for device performance.

High-κ metal-oxides are also required for III-V MOS-devices. Particularly, HfO_2 has been extensively investigated for III-V CMOS applications due to its superior properties, including a high dielectric constant (κ~20-25), a high energy band gap (~6eV) and thermally stable on III-V [5-10~5-13]. In addition, rare-earth oxides (REOs) are also been currently researched as high-κ materials for post-Hafnium oxides due to their promising properties, such as much higher dielectric constant, large energy band-gap and conduction-band offset [5-14]. Among rare-earth oxides, La_2O_3 is the potential candidate due to its very high dielectric constant (κ~27) [5-15]. However, rare-earth oxides can react with III-V compound semiconductors leading to a poor quality of REO/III-V interface, which degrades the device performance. Therefore, an ultra-thin and thermal stable interlayer (IL) between the III-V high mobility channel and the

RE-gate dielectric is needed for the improvement of the device performance.

In this study, we introduced that HfO_2 as the interlayer (IL) between the high indium content $In_XGa_{1-X}As$ channel and the RE-gate dielectric. Thus, La_2O_3/HfO_2/n-$In_XGa_{1-X}As$ MOS-capacitors were fabricated and evaluated, and the device performance was compared to that of MOS-capacitors with a single-layer high-κ gate dielectric.

5.2.2 Experiment

The structures of the n-$In_XGa_{1-X}As$ MOS-capacitors in this study are as shown in Fig. 5-2-1, including n- $In_{0.53}Ga_{0.47}As$ channel, and n-InAs channel. The device structures were grown by molecular beam epitaxy (MBE) on a 3-in n^+-InP substrate. The structure layer of n-$In_{0.53}Ga_{0.47}As$ is 100-nm-thick with Si doping concentration of $5x10^{17}cm^{-3}$. The structure layers of n-InAs device, from bottom to top, are composed of a 10-nm-thick n-$In_{0.53}Ga_{0.47}As$ (Si：$5x10^{17}cm^{-3}$), a 3-nm-thick n-$In_{0.70}Ga_{0.30}As$ (Si：$5x10^{17}cm^{-3}$), and a 5-nm-thick n-InAs (Si：$5x10^{17}cm^{-3}$).

The wafers were first cleaned in a dilute HF (50%) solution for 3 minutes, and then followed by surface treatment in a $(NH_4)_2S_X$ solution for 30 minutes at room temperature. After cleaning, the wafer was deposited bilayer gate dielectric La_2O_3/HfO_2 at 300^oC using the MBE system. For the test samples, pure La_2O_3 or pure HfO_2 was also deposited under the same condition. After the gate oxide deposition, the post deposition annealing (PDA) process was performed at 400 ^oC. Then, W metal was deposited as the gate metal by the lift-off process and Au metal was deposited by the sputtering process as the backside ohmic contact.

Fig. 5-2-1 Structures of the n-$In_XGa_{1-X}As$ MOS-capacitors

5.2.3 Results and Discussion

J_G-V_G Characteristics

Fig. 5-2-2 shows the gate leakage current density of n-$In_{0.53}Ga_{0.47}As$ MOS-capacitors with La_2O_3, HfO_2, and La_2O_3/HfO_2 bilayer gate dielectrics. The La_2O_3 dielectric film exhibited a high leakage current due to the intensive interaction between La_2O_3 and III-V semiconductor, which caused the poor interface quality. And it can be seen that the gate leakage current of the La_2O_3/HfO_2 dielectric film was significantly reduced by the use of a thin HfO_2 interlayer (IL).

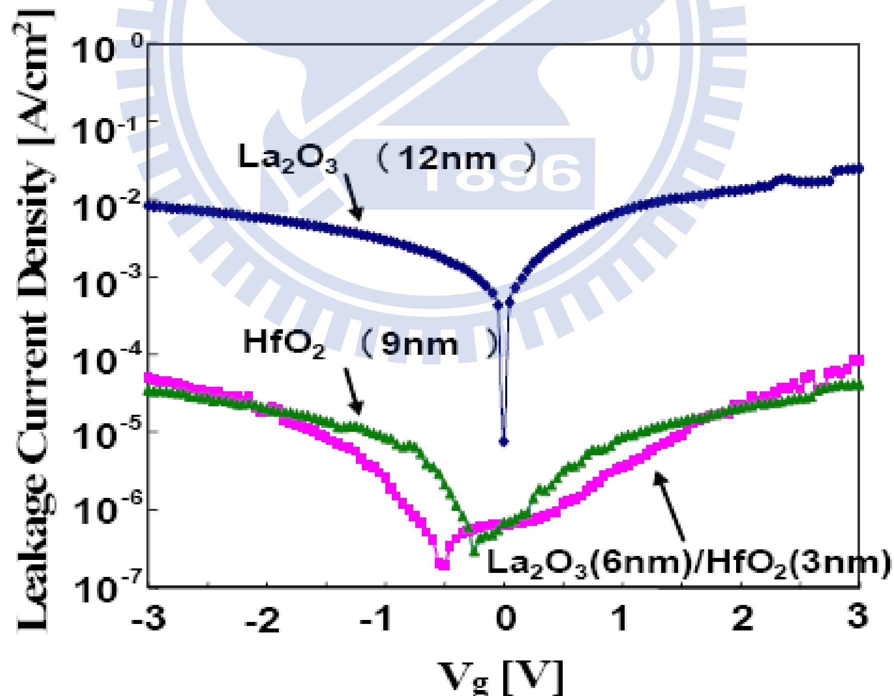

Fig. 5-2-2 Gate leakage current density, J_G-V_G, of La_2O_3, HfO_2, and La_2O_3/HfO_2 n-$In_{0.53}Ga_{0.47}As$ MOS-capacitors

C-V Characteristics

The *C-V* characteristics of n-$In_{0.53}Ga_{0.47}As$ MOS-capacitors with La_2O_3, HfO_2, and La_2O_3/HfO_2 bilayer gate dielectrics were shown in Fig. 5-2-3. The MOS-capacitor with La_2O_3 gate dielectric performed a larger capacitance value at the accumulation than that of HfO_2 one, but both of them had the serious frequency dispersion. The MOS-capacitor with La_2O_3/HfO_2 gate dielectric showed the highest capacitance value as well as the small frequency dispersion.

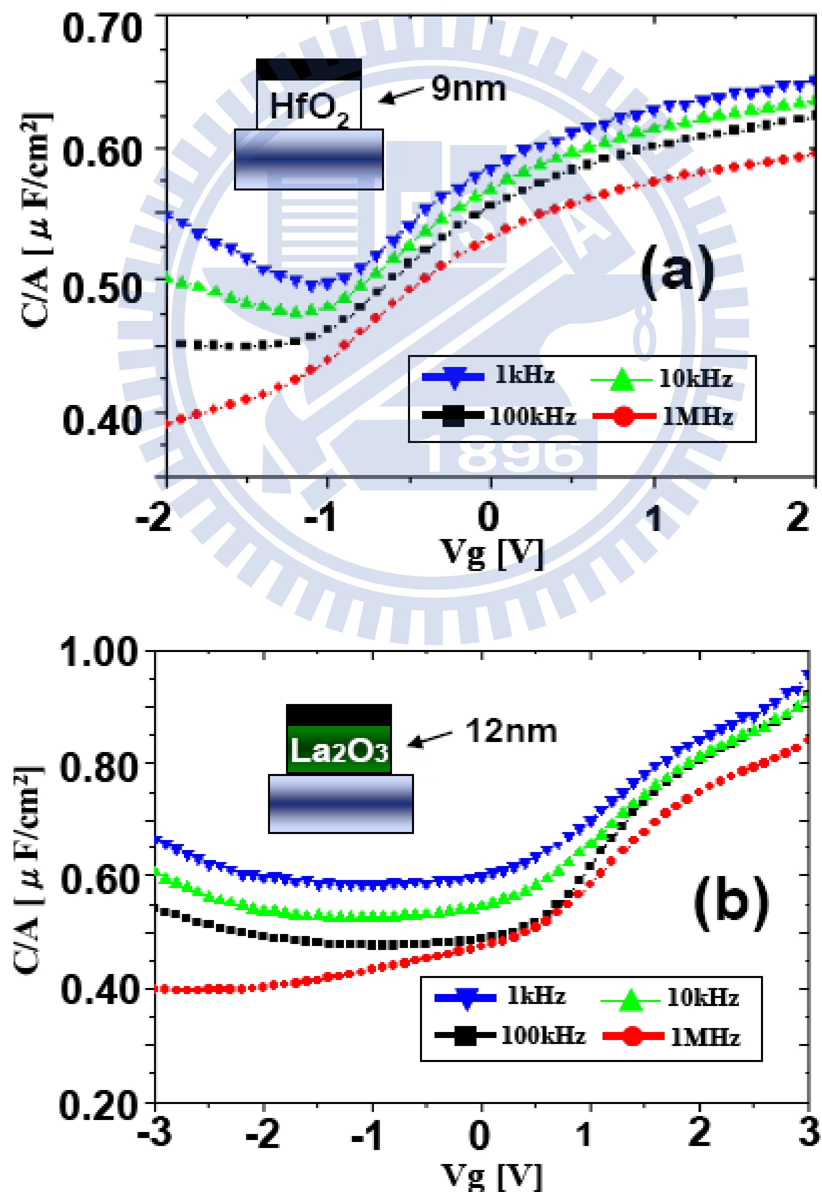

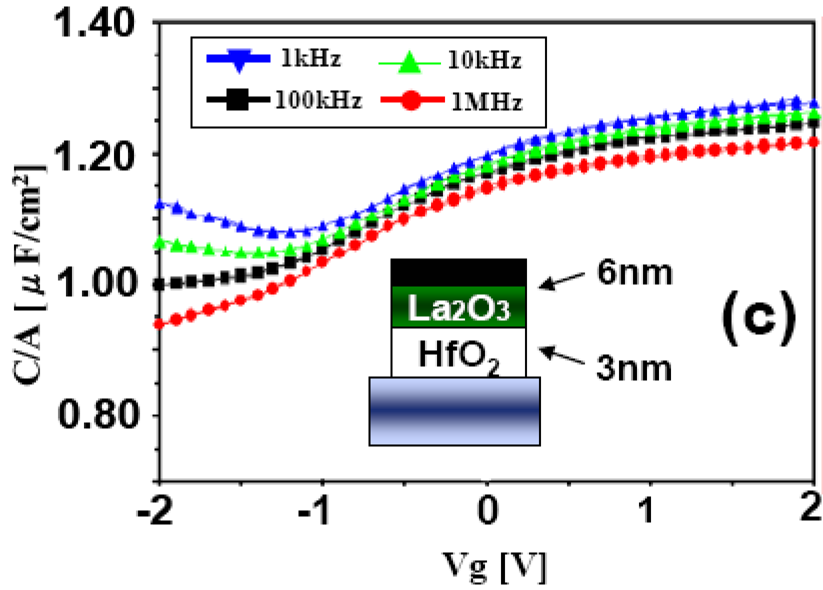

Fig. 5-2-3 *C-V* characteristics of the n-$In_{0.53}Ga_{0.47}As$ MOS-capacitors with the different gate dielectrics (a) HfO_2 (b) La_2O_3 (c) La_2O_3/HfO_2

The *C-V* characteristics of n-InAs MOS-capacitors with HfO_2, and La_2O_3/HfO_2 bilayer gate dielectrics were also investigated and the results are shown in Fig. 5-2-4. Similarly, it showed the same trend that the n-InAs MOS-capacitor with La_2O_3/HfO_2 bilayer gate dielectrics had the highest capacitance value and small frequency dispersion. Furthermore, the *C-V* curve had much stronger inversion characteristics for the InAs-channel capacitor.

The *C-V* characteristics of La_2O_3 (10nm)/HfO_2 (5nm) and HfO_2 (15nm) on n-InAs and p-$In_{0.7}Ga_{0.3}As$ MOS-capacitors at 100kHz were compared and demonstrated in Fig. 5-2-5. It can be seen that the accumulation capacitance value was also enhanced by the use of La_2O_3/HfO_2 bilayer gate dielectrics. As shown in Fig. 5-2-5, the accumulation capacitance was increased from 0.73 (μF/cm^2) of HfO_2/n-InAs capacitor to 1.26 (μF/cm^2) of La_2O_3/HfO_2/n-InAs capacitor, and from 0.50 (μF/cm^2) for HfO_2/p-$In_{0.7}Ga_{0.3}As$ capacitor to 1.05 (μF/cm^2) for La_2O_3/HfO_2/p-$In_{0.7}Ga_{0.3}As$ capacitor.

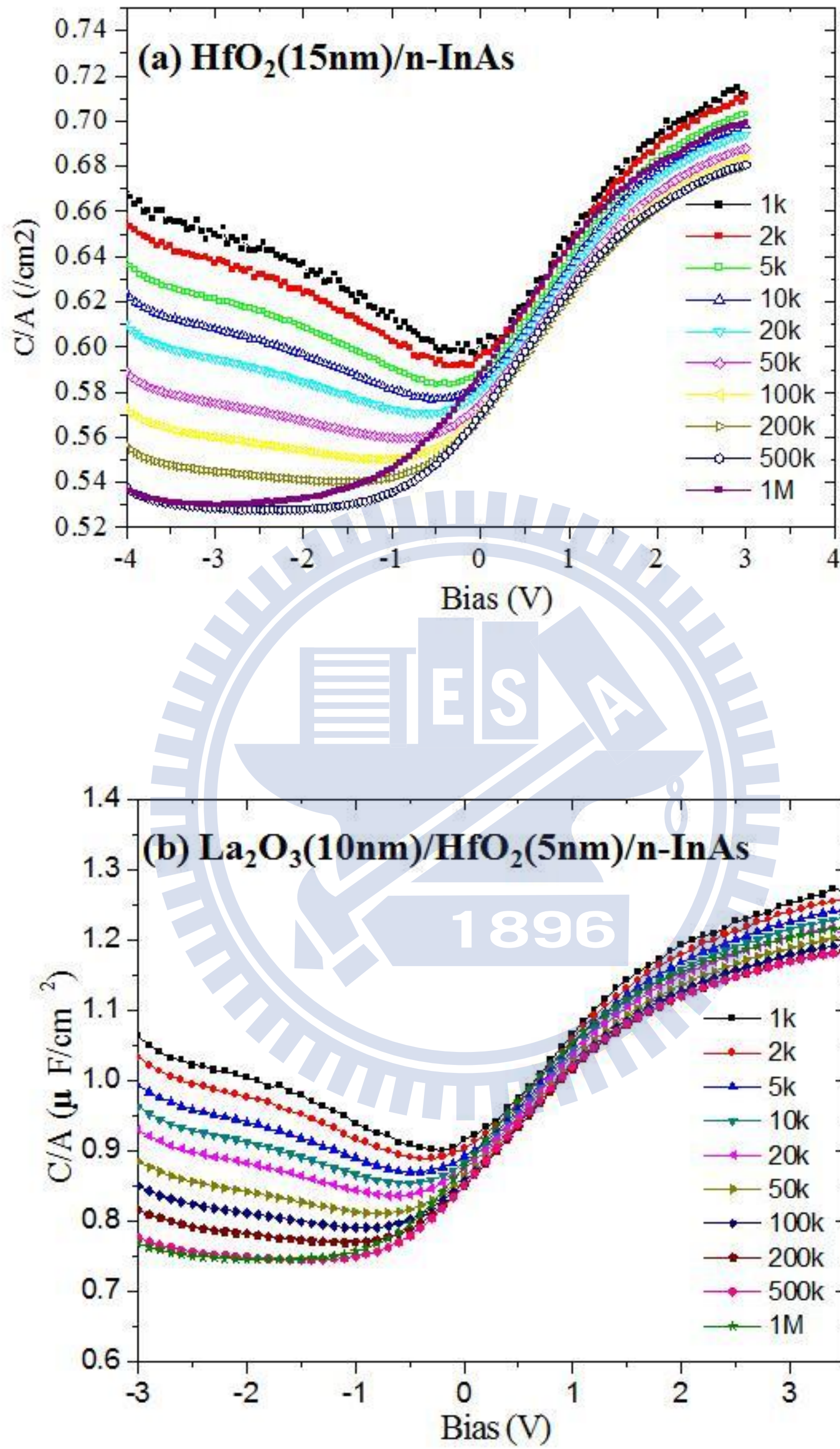

Fig. 5-2-4 *C-V* characteristics of the n-InAs MOS-capacitors with the different gate dielectrics (a) HfO_2 (b) La_2O_3/HfO_2

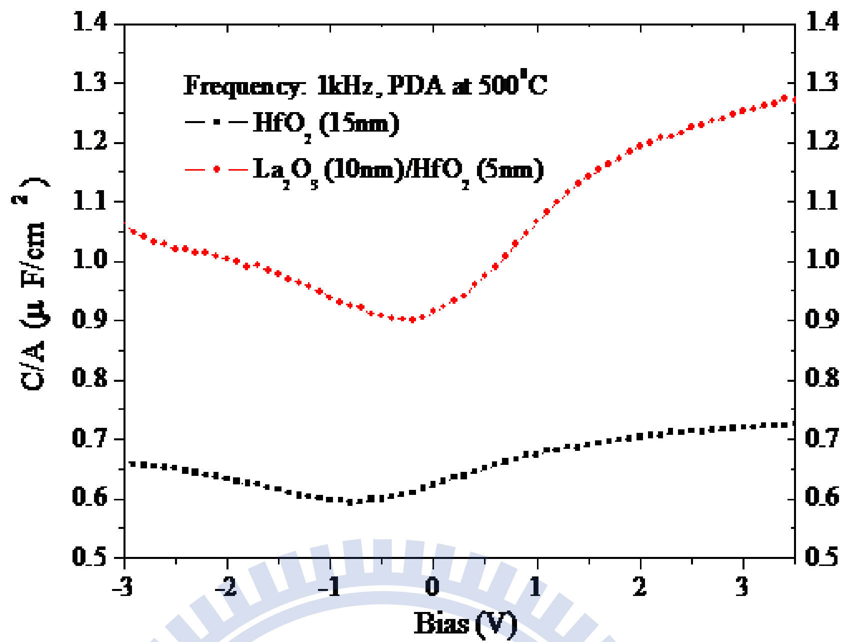

(a) n-InAs MOS-capacitor

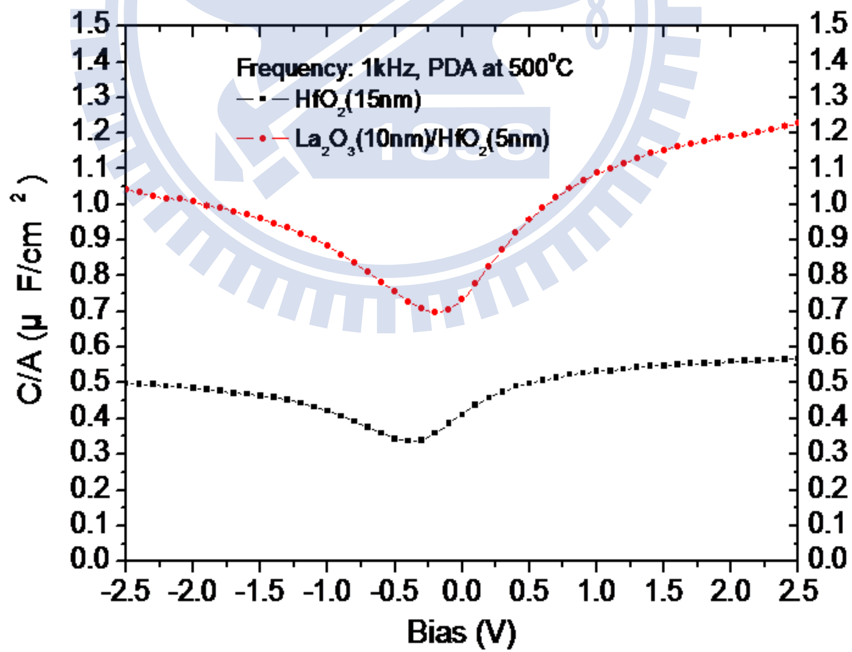

(b) p-$In_{0.7}Ga_{0.3}As$ MOS-capacitor

Fig. 5-2-5 Comparison of *C-V* characteristics at 100kHz of the La_2O_3/HfO_2 and HfO_2 $In_XGa_{1-X}As$ MOS-capacitors (a) n-InAs (b) p-$In_{0.7}Ga_{0.3}As$

5.2.4 Conclusion

In this study, the electrical characteristics of $In_XGa_{1-X}As$ MOS-capacitors were improved by the use of bilayer gate dielectrics composed of a rare-earth oxide and a thin HfO_2 interlayer (IL).

The use of a thin interlayer reduces the leakage current for the $La_2O_3/HfO_2/n-In_{0.53}Ga_{0.47}As$ MOS-capacitor, which is much smaller compared to the La_2O_3 one, and it had a higher accumulation capacitance value compared to the HfO_2 one. By replacing $In_{0.53}Ga_{0.47}As$ with InAs, the inversion behavior of *C-V* curve was much stronger due to the much higher carrier mobility of InAs. The capacitance increased at the accumulation region due to the addition of La_2O_3 as compared to the pure $HfO_2/In_XGa_{1-X}As$ MOS-capacitor. The capacitance value increased from 0.73 ($\mu F/cm^2$) to 1.26 ($\mu F/cm^2$) for the n-InAs MOS-capacitor, and from 0.5 ($\mu F/cm^2$) to 1.05 ($\mu F/cm^2$) for the $p-In_{0.7}Ga_{0.3}As$ MOS-capacitor.

5.3 Effect of Thermal Treatment on Properties of HfO_2/p-$In_{0.7}Ga_{0.3}As$ Metal-Oxide-Semiconductor Capacitors

5.3.1 Introduction

Si-based complementary metal-oxide-semiconductor (CMOS) devices with traditional structures are approaching the theoretical limit. One of the research trend for advanced very-large-scale-integrated circuits (VLSIs) in digital applications beyond 22 nm node is using III-V compound semiconductors as channel material to replace traditional Si or strained Si, and integrating metal gates and high-κ dielectrics with these high-mobility materials [5-16]. However, the lack of high quality and thermally stable gate dielectrics on III-V channel materials causes a high surface trap density (D_{it}) and serious Fermi level pinning phenomenon, which remains the main obstacle to realize III-V MOS-technology for commercial. Currently, a lot of approaches were tried to improve the dielectric/III-V interface qualities, which include silicon interface control layers (Si-ICLs) [5-17~5-19], sulfer passivation [5-20~5-21], *in-situ* molecular-beam-epitaxy (MBE) grow of Gd_2O_3/Ga_2O_3 [5-22], *ex-situ* atomic layer deposition (ALD) growth of Al_2O_3 and HfO_2 [5-23~5-24], and nitride-based materials as interlayers (ILs) [5-25~5-29].

HfO_2 has a high dielectric constant (κ~20-25) with a high energy bandgap (~6eV) and is considered as a potential high-κ material for next generation CMOS logic applications. The effect of thermal treatment on the electrical characteristics of the HfO_2/p-$In_{0.7}Ga_{0.3}As$ MOS-capacitor is investigated in this study.

5.3.2 Experiment

The structure of the p-$In_{0.7}Ga_{0.3}As$ MOS-capacitor in this study is as shown in Fig. 5-3-1, and the wafer structure was grown by molecular beam epitaxy (MBE) on a 3-in p^+-InP substrate. The structure layers, from bottom to top, composed of a 50-nm-thick p-$In_{0.53}Ga_{0.47}As$ (Be：$5x10^{17}cm^{-3}$), and a 20-nm-thick p-$In_{0.70}Ga_{0.30}As$ (Be：$5x10^{17}cm^{-3}$).

The wafers were first cleaned in a dilute HF (50%) solution for 3 minutes, and then followed by surface treatment in a $(NH_4)_2S_X$ solution for 30 minutes at room temperature. The HfO_2 was deposited at 300°C by the MBE system followed by the thermal treatment. The two-steps annealing process was performed by the first step annealing after a thin 5nm HfO_2 layer was deposited and the second step lower temperature annealing was performed after another 10nm HfO_2 was deposited. For the test sample, one-step annealing process was also performed. Then, tungsten (W) metal (contact size: 50μm in diameter) was deposited as the gate metal by the lift-off process and gold (Au) metal was deposited by the sputtering process as the backside ohmic contact.

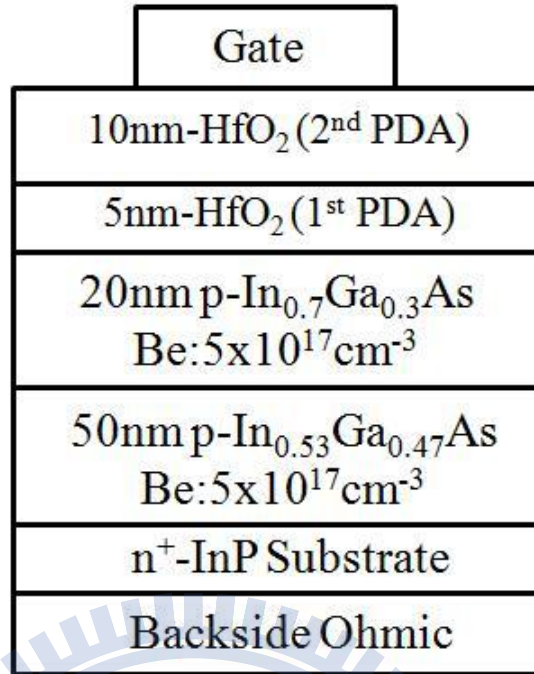

Fig. 5-3-1 Structure of the HfO_2/p-$In_{0.7}Ga_{0.3}As$ MOS-capacitor with the two-steps annealing process

5.3.3 Results and Discussion

Table 5-3-1 shows the hysteresis behaviors of HfO_2(5nm)/p-$In_{0.7}Ga_{0.3}As$ MOS-capacitors at the different first step post deposition annealing (PDA) temperatures. It can be seen that the device at the PDA temperature of 400°C had a large hysteresis value (ΔV=247 mV), and the hysteresis value was decreased with the increase of the first step annealing temperature to 500°C. It implied that the quality of HfO_2 film was improved with a higher PDA temperature. However, when the PDA temperature was over 500°C, a small amount of indium (In) diffused into HfO_2, which resulted in the increase of In-oxide defects.

The interface-trap densities (D_{it}) of devices at the different first step PDA temperatures were estimated by the conductance method as also listed in the Table 5-3-1. It shows that the device at a higher PDA temperature had a lower

D_{it} value and also means that the quality of oxide/semiconductor interface was improved after a higher annealing temperature. The comparisons of hysteresis and interface trap density (D_{it}) after thermal annealing at the different temperatures are shown in Fig. 5-3-2.

Table 5-3-1 Comparison of interface trap density (D_{it}) and hysteresis of the HfO_2/p-$In_{0.7}Ga_{0.3}As$ MOS-capacitors at the different first step PDA temperatures

PDA temp. (^oC)	400	450	500	550
Hysteresis (mV)	247	146	182	421
D_{it} ($cm^{-2}e\cdot V^{-1}$)	3.43 x10^{13}	1.8 x10^{13}	1.3x10^{13}	1.7x10^{13}

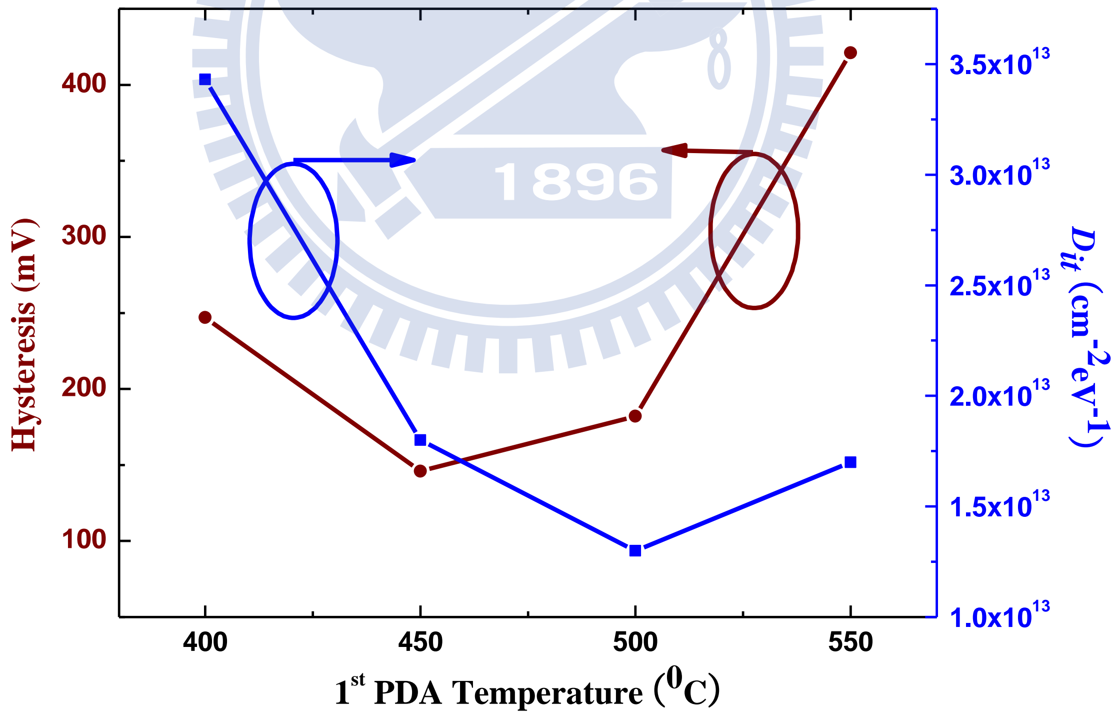

Fig. 5-3-2 Comparison of interface trap density (D_{it}) and hysteresis of the HfO_2/p-$In_{0.7}Ga_{0.3}As$ MOS-capacitors at the different first step PDA temperatures

Based on the discussion above, the optimum first step annealing temperature was in the range of 450°C~500°C. Thus, 450°C and 500°C were chose as the first step annealing temperatures. For the sample with the first step PDA temperature at 450°C, the second step annealing temperatures included 400°C, and 450°C. The interface trap densities (D_{it}) and hysteresis were measured again after the second step annealing as shown in Table 5-3-2, and compared in Fig. 5-3-3. It can be seen that the quality of oxide/semiconductor and oxide were further improved by the second step annealing due to the decrease of D_{it} and hysteresis value.

The *C*-*V* characteristics of HfO_2/p-$In_{0.7}Ga_{0.3}As$ MOS-capacitors with the first step annealing at 450°C and the different second step annealing temperatures were compared and shown in Fig. 5-3-4. The frequency dispersion and the hysteresis behavior were all improved with the two-steps annealing process.

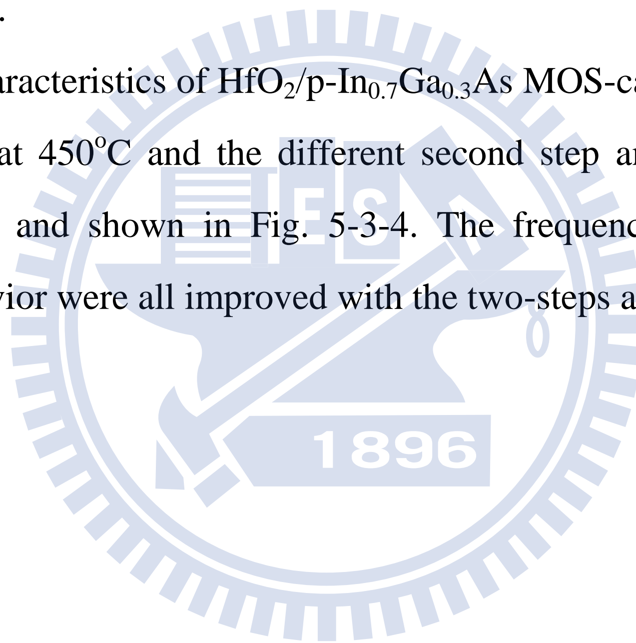

Table 5-3-2 Comparison of interface trap density (D_{it}) and hysteresis of the HfO_2/p-$In_{0.7}Ga_{0.3}As$ MOS-capacitors with the first step annealing at 450°C and the different second step annealing temperatures

1st PDA (°C)	450	450	450
2nd PDA (°C)	0	400	450
D_{it} ($cm^{-2}eV^{-1}$)	1.8 $\times 10^{13}$	3.61 $\times 10^{12}$	3.69 $\times 10^{12}$
Hysteresis (mV)	146	69	128

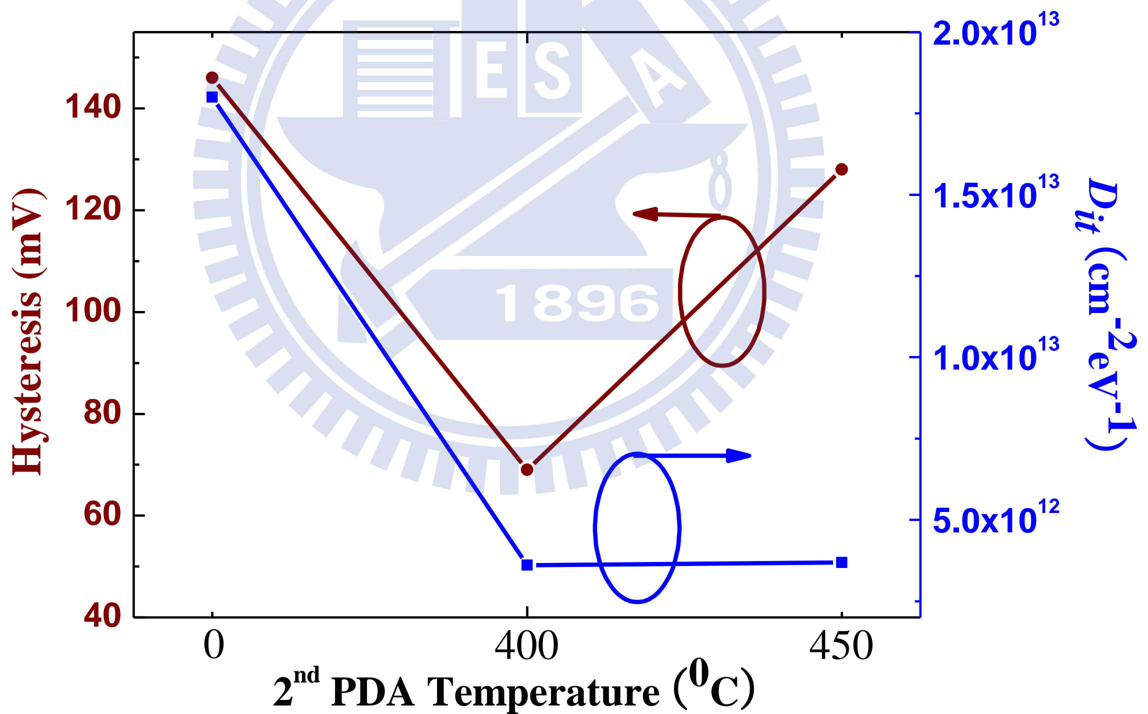

Fig. 5-3-3 Comparison of interface trap density (D_{it}) and hysteresis of the HfO_2/p-$In_{0.7}Ga_{0.3}As$ MOS-capacitors with the first step annealing at 450°C and the different second step annealing temperatures

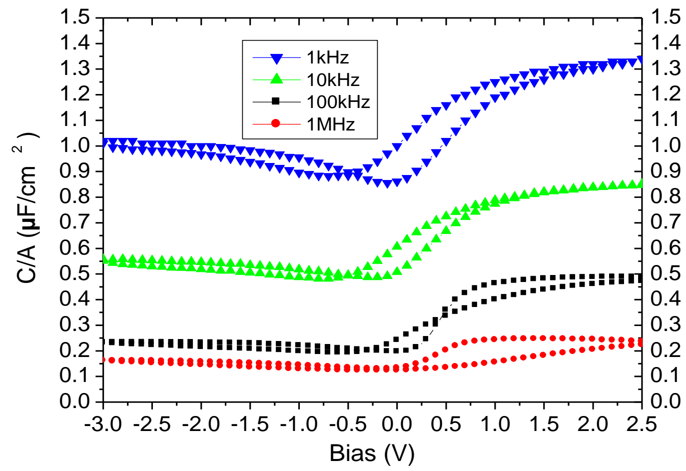

(a) 450°C

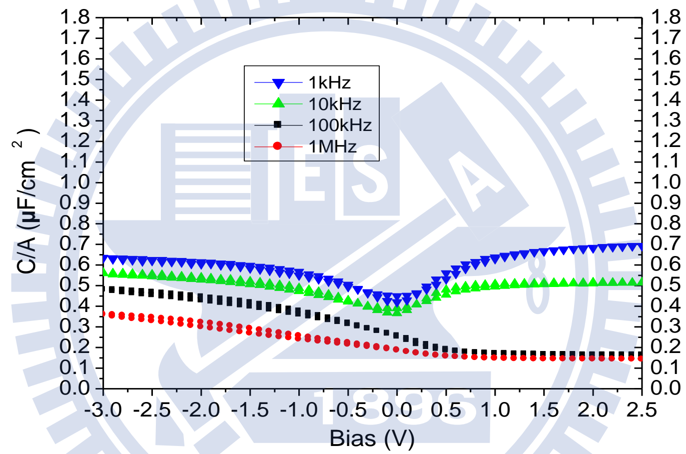

(b) 450°C/400°C

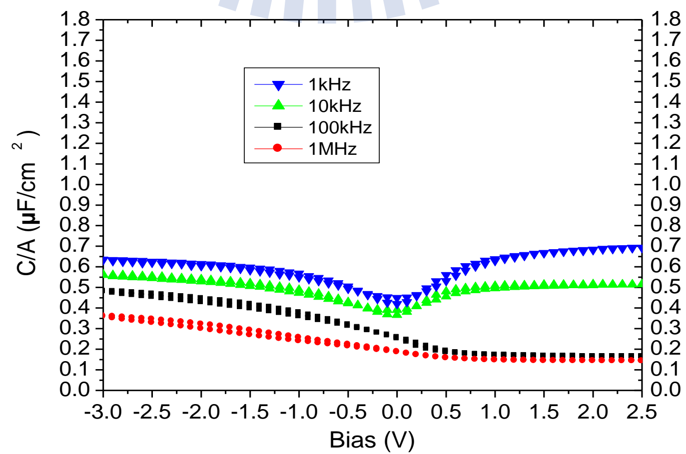

(c) 450°C/450°C

Fig. 5-3-4 *C-V* characteristics of the HfO_2/p-$In_{0.7}Ga_{0.3}As$ MOS-capacitors with the first step annealing at 450°C and the different second step annealing temperatures

For the sample with the first step PDA temperature at 500°C, the second step annealing temperatures included 400°C, 450°C, and 500°C. The interface trap densities (D_{it}) and hysteresis were measured again after the second step annealing process, and the results are shown in Table 5-3-3, and compared in Fig. 5-3-5. It can be seen that the quality of oxide/semiconductor interface and the oxide quality were also further improved by the second step annealing as evidenced by the decrease of D_{it} and hysteresis value except for the sample with the second step annealing at 400°C.

The *C-V* characteristics of HfO_2/p-$In_{0.7}Ga_{0.3}As$ MOS-capacitors with the first step 500°C annealing and the different second step annealing temperatures were compared and the results are shown in Fig. 5-3-6. The frequency dispersion and the hysteresis behavior were all also improved with the two-steps annealing process except the one with the second step annealing at 400°C.

The reason for the device performance degradation after the 500°C/400°C two-steps annealing process was believed to be that there was a large lattice mismatch between the two HfO_2 layers because the crystal structure of HfO_2 is amorphous after 400°C annealing, and is tetragonal after 500°C annealing. Because of a large lattice mismatch between these two HfO_2 layers, a small amount of additional defects existed at the interface of oxides which degraded the device performance, including a higher D_{it} and hysteresis value.

Finally, it is observed that the best *C-V* characteristics of HfO_2/p-$In_{0.7}Ga_{0.3}As$ MOS-capacitor could be achieved after the first PDA temperature of 450°C and the second PDA temperature of 400°C was used.

Table 5-3-3 Comparison of interface trap density (D_{it}) and hysteresis of the HfO_2/p-$In_{0.7}Ga_{0.3}As$ MOS-capacitors with the first step annealing at 500°C and the different second step annealing temperatures

1st PDA (^{o}C)	500	500	500	500
2nd PDA (^{o}C)	0	400	450	500
D_{it} ($cm^{-2}e\cdot V^{-1}$)	$1.3x10^{13}$	$1.65\ x10^{13}$	$3.35\ x10^{12}$	$4.71\ x10^{12}$
Hysteresis (mV)	182	376	139	121

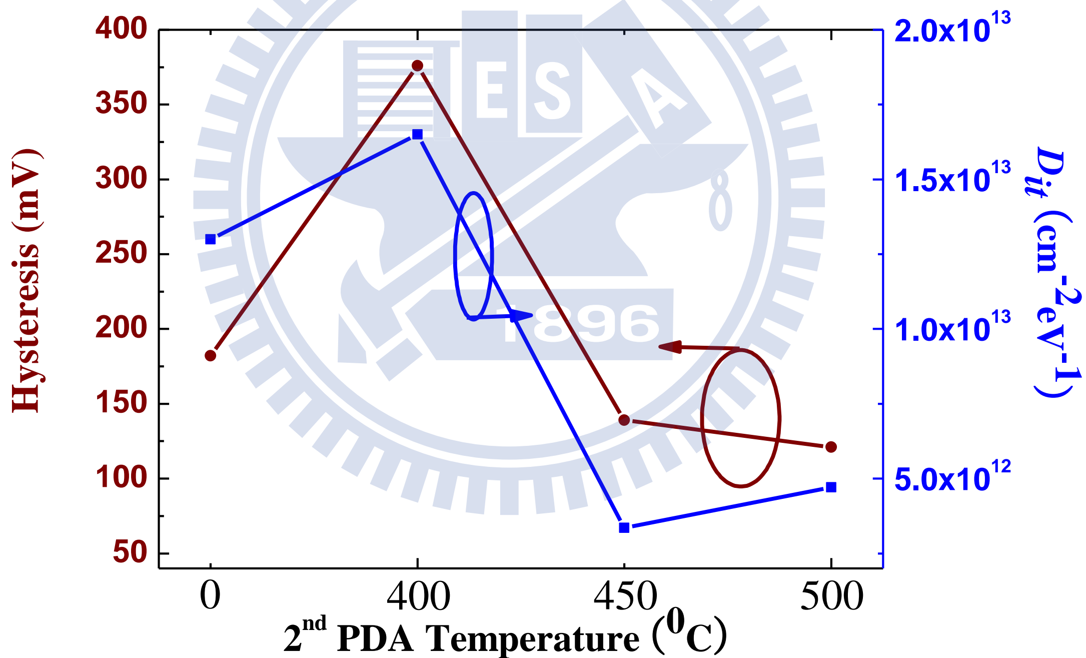

Fig. 5-3-5 Comparison of interface trap density (D_{it}) and hysteresis of the HfO_2/p-$In_{0.7}Ga_{0.3}As$ MOS-capacitors with the first step annealing at 500°C and the different second step annealing temperatures

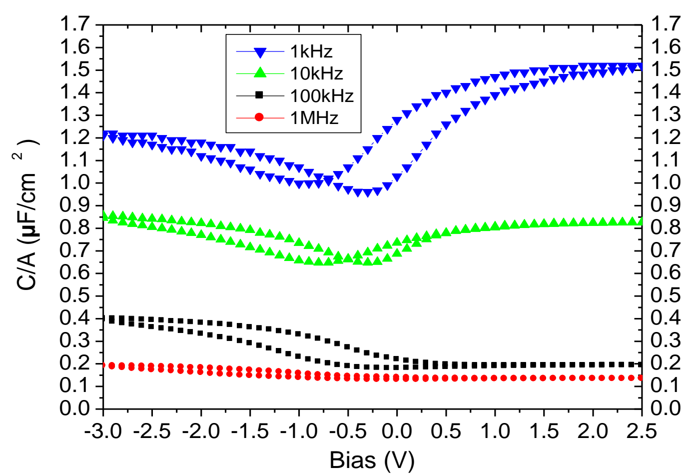

(a) 500°C

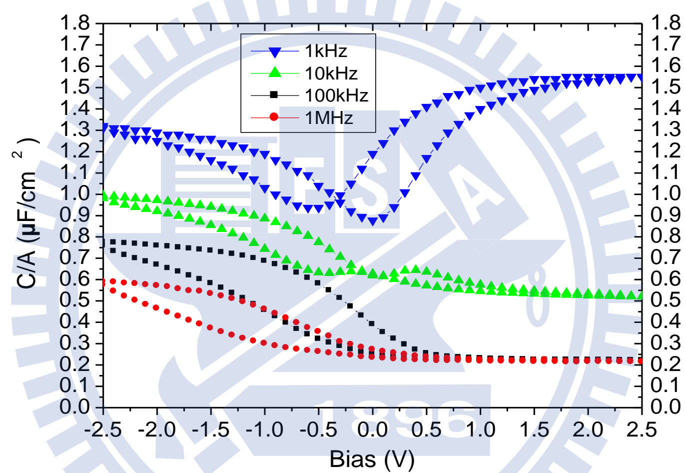

(b) 500°C/400°C

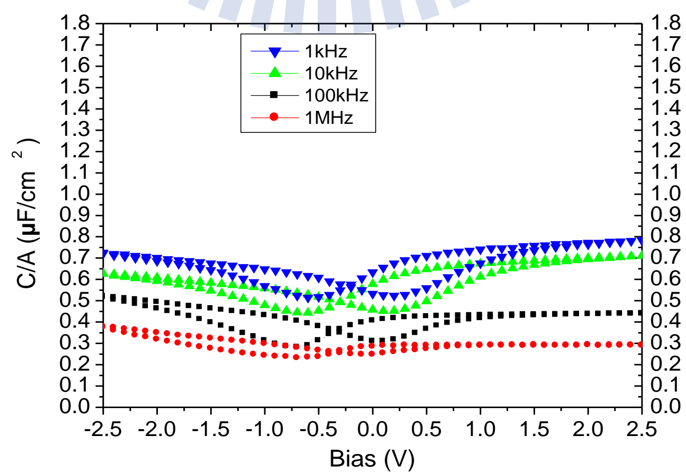

(c) 500°C/450°C

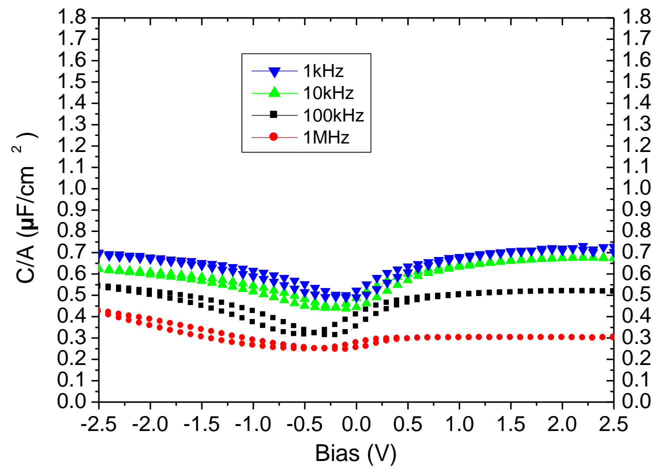

(d) $500^{o}C/500^{o}C$

Fig. 5-3-6 *C-V* characteristics of the $HfO_2/p\text{-}In_{0.7}Ga_{0.3}As$ MOS-capacitors with the first step annealing at $500^{o}C$ and the different second step annealing temperatures

5.3.4 Conclusion

$HfO_2/p\text{-}In_{0.7}Ga_{0.3}As$ MOS-capacitors with the different two-steps post deposition annealing (PDA) processes were investigated. With the increase of first PDA temperature, the defects at the oxide/semiconductor interface were reduced, and the oxide quality was improved. However, a higher annealing temperature over $500^{o}C$ would cause a small amount of indium (In) out-diffusing into HfO_2, which degraded the device performance.

Two-steps PDA process would result in device with a small frequency dispersion and hysteresis. The *C-V* characteristics would be improved after the second annealing. The experiment results also showed that a large temperature difference between the first step and the second step would cause the more serious hysteresis due to a large lattice mismatch between the two HfO_2 layers. Overall, the first PDA temperature at $450^{o}C$ and the second PDA temperature at $400^{o}C$ achieved the best device performance.

Chapter 6

Conclusion

III-V MOS-capacitors with the $In_XGa_{1-X}As$ channel and the high-κ gate dielectric are investigated in this study. By using the high-κ materials (HfO_2, and La_2O_3), the high indium (In) content $In_XGa_{1-X}As$ channel, and the proper thermal treatment, the performance of the III-V MOS-capacitors are improved.

The HfO_2/n-InAs MOS-capacitor shows the best electrical characteristics after the 500°C PDA annealing due to the optimized oxide/semiconductor interface quality with a low interface trap density (D_{it}) value after the annealing. In addition, the device performance degraded when the annealing temperature was over 500°C because a small amount of indium (In) atoms diffused into the HfO_2 layer with the increase of In-oxide defects formation.

Even though rare-earth oxides have higher dielectric constants, their capacitors exhibit a large gate leakage current compared to HfO_2 one due to the difference of interfacial interactions between oxide and substrate. After annealing, some of the atoms from the substrate diffused into the RE-oxide gate dielectric, however, the diffusion of atoms from the substrate was suppressed due to the use of HfO_2 diffusion barrier layer. Thus, inserting a thin HfO_2 interlayer between the RE-oxide and the substrate as bilayer gate dielectrics was useful to improve the device performance such as decreasing the gate leakage current and enhancing the capacitance value with small frequency dispersion. Moreover, the high indium (In) content $In_XGa_{1-X}As$ channel used could also result in the better *C-V* characteristics.

The two-steps thermal annealing process was useful for the enhancement of the device performance. The first step annealing with a higher temperature was used to improve the oxide/semiconductor interface quality resulting in a low interface trap density (D_{it}) value. The second annealing with a lower temperature was performed to obtain a small hysteresis effect as well as a much lower D_{it} value. However, a small temperature difference between the two steps annealing was needed to prevent a large lattice mismatch between the two oxide layers which resulted in additional defects at the interface of the two oxides.

Reference

Chapter 1

[1-1] Mark T. Bohr, "Nanotechnology Goals and Challenges for Electronic Applications" *IEEE Transactions on Nanotechnology, vol. 1, no. 1, March 2002*

[1-2] Robert Chau, Justin Brask, Suman Dana, Gilbert Dewey, Mark Doczy, Brian Doyle, Jack Kavalieros, Ben Jin, Matthew Metz, Amlan Majumdar, and Marko Radosavljevic, "Emerging Silicon and Non-Silicon Nanoelectronic Devices: Opportunities and Challenges for Future High-Performance and Low-Power Computational Applications (Invited Paper)"

[1-3] Robert Chau, Suman Datt, Mark Doczy, Brian Doyle, Ben Jin, Jack Kavalieros, Amlan Majumdar, Matthew Metz, and Marko Radosavljevic, "Benchmarking Nanotechnology for High-Performance and Low-Power Logic Transistor Applications" *IEEE Transactions on Nanotechnology, vol. 4, no. 2, March 2005*

[1-4] Y. Q. Wu, W. K. Wang, O. Koybasi, D. N. Zakharov, E. A. Stach, S. Nakahara, J. C. M. Hwang, P. D. Ye, "0.8-V Supply Voltage Deep-Submicrometer Inversion-Mode $In_{0.75}Ga_{0.25}As$ MOSFET," *IEEE Electron Device Letters, vol. 30, no. 7, July 2009*

[1-5] P.D. Ye, Y. Xuan, Y.Q. Wu, and M. Xu, "Inversion-mode $In_xGa_{1-x}As$ MOSFETs (x=0.53, 0.65, 0.75) with atomic-layerdeposited high-κ dielectrics," *ECS Transactions, 19 (2) 605-614 (2009)*

[1-6] Ning Li, Eric S. Harmon, James Hyland, David B. Salzman, T. P. Ma, Yi Xuan, and P. D. Ye, "Properties of InAs metal-oxide-semiconductor structures with atomic-layer deposited Al_2O_3 Dielectric," *Applied Physics Letters* ***92****, 143507*

(2008)

[1-7] Mo Wu, Y. I. Alivov, and Hadis Morkoc, "High-κ dielectrics and advanced channel concepts for Si MOSFET," *J Mater Sci: Mater Electron (2008) 19:915–951*

Chapter 2

[2-1] Donald A. Neamen, "Semiconductor Physics & Devices," *third edition*

[2-2] G. E. Moore, "Progress in digital integrated circuit," *IEDM Tech. Dig., pp. 11-13, 1975*

[2-3] G. E. Moore, "Microprocessors and integrated electronic technology," *Proceedings of the IEEE, vol. 64, no. 6, pp. 837-841, June 1976*

[2-4] Robert H. Dennard, Fritz H. Gaensslen, Hwa-Nien Yu, V. Leo Rideout, Ernest Bassous, and Andre R. Leblanc, "Design of Ion-Implanted MOSFET's with Very Small Physical Dimensions," *Proceedings of the IEEE, vol. 87, no. 4, April 1999*

[2-5] Mo Wu, Y. I. Alivov, and Hadis Morkoc, "High-κ dielectrics and advanced channel concepts for Si MOSFET," *J Mater Sci: Mater Electron (2008) 19:915–951*

[2-6] Martin von Haartman, B. Gunnar Malm, Mikael Östling, "Comprehensive Study on Low-Frequency Noise and Mobility in Si and SiGe pMOSFETs With High-κ Gate Dielectrics and TiN Gate," *IEEE Transactions on Electron Devices, vol. 53, no. 4, April 2006*

[2-7] M. Xu, Y. Q. Wu, O. Koybasi, T. Shen, and P. D. Ye, "Metal-oxide-semiconductor field-effect transistors on GaAs (111)A surface

with atomic-layer-deposited Al_2O_3 as gate dielectrics," *Applied Physics Letters 94, 212104 (2009)*

[2-8] H. C. Lin, T. Yang, H. Sharifi, S. K. Kim, Y. Xuan, T. Shen, S. Mohammadi, and P. D. Ye, "Enhancement-mode GaAs metal-oxide-semiconductor high-electronmobility transistors with atomic layer deposited Al_2O_3 as gate dielectric," *Applied Physics Letters 91, 212101 (2007)*

[2-9] P. D. Ye, B. Yang, K. K. Ng, J. Bude, G. D. Wilk, S. Halder and J. C. M. Hwang, "GaN metal-oxide-semiconductor high-electron-mobility-transistor with atomic layer deposited Al_2O_3 as gate dielectric," *Applied Physics Letters 86, 063501 (2005)*

[2-10] Shankar Swaminathan, Michael Shandalov, Yasuhiro Oshima, and Paul C. McIntyre, "Bilayer metal oxide gate insulators for scaled Ge-channel metal-oxide-semiconductor devices," *Applied Physics Letters 96, 082904 (2010)*

[2-11] Shreyas Y. Shah, "Rare-earth Oxides For Post-Hafnium Oxide CMOS Era"

[2-12] Sabina Spiga, Claudia Wiemer, Giovanna Scarel, Omar Costa, and Marco Fanciulli, "Electrical Characterization of Rare Earth Oxides Grown by Atomic Layer Deposition"

[2-13] Y. Taur and T. Ning, "Fundamentals of Modern VLSI devices," *Cambridge, 1998. Chapter 3-2*

[2-14] S. Tiwari et al., "Hole mobility improvement in silicon-on-insulator and bulk silicon transistors using local strain," *IEDM Tech. Dig., pp. 939-41, 1997*

[2-15] A. Shimizu et al., "Local mechanical-stress control (LMC): a new technique for CMOS-performance enhancement," *IEDM Tech. Dig., pp. 433-436, 2001*

[2-16] K. Ota et al., "Novel locally strained channel technique for high performance 55nm CMOS," *IEDM Tech. Dig., pp. 27-30, 2002*

Chapter 3

[3-1] Website of Dr. Hiroshi Iwai's Lab, Frontier Research Center, Tokyo Institute of Technology

Chapter 4

[4-1] Jaeyeol Song, "A Study on Gate-stack Process for Ge MOS Devices with La2O3 Gate Dielectric,"

[4-2] E.H. Nicollian and A. Goetzberger, "The Si-SiO2 Interface-Electrical Properties as Determined by the Metal-Insulator-Silicon Conductance Technique," *Bell Syst. Tech. J., vol.46, pp.1055 (1967)*

Chapter 5

[5-1] Yanning Sun, E. W. Kiewra, J. P. De Souza, S. J. Koester, J. J. Bucchignano, N. Ruiz, K. E. Fogel, D. K. Sadana, G. G. Shahidi, J. Fompeyrine, D. J. Webb, M. Sousa, C. Marchiori, R.Germann, and K. T. Shiu, "High mobility III-V Channel MOSFETs for Post-Si CMOS Applications," *2009 IEEE*

[5-2] Abigail Lubow, Sohrab Ismail-Beigi, and T. P. Ma, "Comparison of drive currents in metal-oxide-semiconductor field-effect transistors made of Si, Ge, GaAs, InGaAs, and InAs channels," *Applied Physics Letters 96, 122105 (2010)*

[5-3] Heng-Tung Hsu, Chien-I Kuo, Edward Y. Chang, Fang-Yao Kuo, "Improvement on the noise performance of InAs-based HEMTs with gate

sinking technology," *Microelectronic Engineering 87 (2010) 2253–2257*

[5-4] Chia-Yuan Chang,a Heng-Tung Hsu,b Edward Yi Chang,a,z Hai-Dang Trinh,a and Yasuyuki Miyamoto, "InAs-Channel Metal-Oxide-Semiconductor HEMTs with Atomic-Layer-Deposited Al_2O_3 Gate Dielectric," *Electrochemical and Solid-State Letters, 12 (12)H456-H459 (2009)*

[5-5] Mo Wu, Y. I. Alivov, and Hadis Morkoc, "High-κ dielectrics and advanced channel concepts for Si MOSFET," *J Mater Sci: Mater Electron (2008) 19:915–951*

[5-6] Marko Milojevic, Christopher L. Hinkle, Eric M. Vogel and Robert M. Wallace, "Interfacial Chemistry of Oxides on III-V Compound Semiconductors," *Chapter 6*

[5-7] Yun-Chi Wua, Edward Yi Chang, Yueh-Chin Lin, Chi-Chung Kei, Mantu K. Hudait , Marko Radosavljevic , Yuen-Yee Wong, Chia-Ta Chang, Jui-Chien Huang, Shih-Hsuan Tang, "Study of the inversion behaviors of $Al_2O_3/In_XGa_{1-X}As$ metal–oxide–semiconductor capacitors with different In contents," *Solid-State Electronics 54 (2010) 37–41*

[5-8] P.D. Ye, Y. Xuan, Y.Q. Wu, and M. Xu, "Inversion-mode $In_xGa_{1-x}As$ MOSFETs (x=0.53,0.65,0.75) with atomic-layer-deposited high-κ dielectrics," *ECS Transactions, 19 (2) 605-614 (2009)*

[5-9] Y. Xuan, T. Shen, M. Xu, Y.Q. Wu, and P. D. Ye, "High-performance Surface Channel In-rich $In_{0.75}Ga_{0.25}As$ MOSFETs with ALD High-κ as Gate Dielectric," *2008 IEEE*

[5-10] Han Zhao, Jung Hwan Yum, Yen-Ting Chen, and Jack C. Lee, "$In_{0.53}Ga_{0.47}As$ *n*-metal-oxide-semiconductor field effect transistors with atomic layer deposited Al_2O_3, HfO_2, and $LaAlO_3$ gate dielectrics," *J. Vac. Sci. Technol. B 27(4), Jul/Aug 2009*

[5-11] Yen-Ting Chen, Han Zhao, Jung Hwan Yum, Yanzhen Wang, and Jack C. Lee, " Metal-oxide-semiconductor field-effect-transistors on indium phosphide using HfO_2 and silicon passivation layer with equivalent oxide thickness of 18 Å," *Applied Physics Letters 94, 213505 (2009)*

[5-12] Y. Xuan, Y. Q. Wu, T. Shen, T. Yang, and P. D. Ye, "High performance submicron inversion-type enhancement-mode InGaAs MOSFETs with ALD Al_2O_3, HfO_2 and HfAlO as gate dielectrics," *2007 IEEE*

[5-13] S. J. Koester, E. W. Kiewra, Yanning Sun, D. A. Neumayer, J. A. Ott, D. K. Sadana, D. J. Webb, J. Fompeyrine, J.-P. Locquet, M. Sousa, and R. Germann, "Charge trapping and wearout characteristics of self-aligned enhancement-mode GaAs n-MOSFET with Si interface passivation layer and HfO_2 gate oxide," *2008 IEEE*

[5-14] Shreyas Y. Shah, "Rare-earth Oxides For Post-Hafnium Oxide CMOS Era"

[5-15] Sabina Spiga, Claudia Wiemer, Giovanna Scarel, Omar Costa, and Marco Fanciulli, "Electrical Characterization of Rare Earth Oxides Grown by Atomic Layer Deposition," *M. Fanciulli, G. Scarel (Eds.): Rare Earth Oxide Thin Films, Topics Appl. Physics 106, 203–223 (2007)*

[5-16] Robert Chau, Suman Datta, and Amlan Majumdar, "Opportunities and Challenges of III-V Nanoelectronics for Future High-Speed, Low-Power Logic Applications," *2005 IEEE*

[5-17] M. Akazawa, H. Hasegawa, "High-κ Al_2O_3 MOS structures with Si interface control layer formed on air-exposed GaAs and InGaAs wafers," *Appli ed Surface Science 256 (2010) 5708–5713*

[5-18] M. Akazawa, H. Hasegawa, "Optimization of Si interface control layer thickness for high-κ GaAs metal–insulator–semiconductor structures," *Materials Science and Engineering B 165 (2009) 122–125*

[5-19] Masamichi Akazawa, Alina Domanowska, Boguslawa Adamowicz, and Hideki Hasegawa, "Capacitance-voltage and photoluminescence study of high-κ/GaAs interfaces controlled by Si interface control layer," *J. Vac. Sci. Technol. B, Vol. 27, No. 4, Jul/Aug 2009*

[5-20] F. S. Aguirre-Tostado, M. Milojevic, K. J. Choi, H. C. Kim, C. L. Hinkle, E. M. Vogel, J. Kim, T. Yang, Y. Xuan, P. D. Ye, and R. M. Wallace, "S passivation of GaAs and band bending reduction upon atomic layer deposition of HfO_2/Al_2O_3 nanolaminates," *Applied Physics Letters 93, 061907 (2008)*

[5-21] E. O'Connor, R. D. Long, K. Cherkaoui, K. K. Thomas, F. Chalvet, I. M. Povey, M. E. Pemble, and P. K. Hurley, B. Brennan and G. Hughes, and S. B. Newcomb, "*In situ* H_2S passivation of $In_{0.53}Ga_{0.47}As$/InP metal-oxide-semiconductor capacitors with atomic-layer deposited HfO_2 gate dielectric," *Applied Physics Letters 92, 022902 (2008)*

[5-22] M. Passlack, M. Hong, and J. P. Mannaerts, "Quasi-static and high frequency capacitance–voltage characterization of Ga_2O_3-GaAs structures fabricated by in-situ molecular beam epitaxy," *Appl. Phys. Lett., vol. 68, no. 8, pp. 1099–1101, Feb. 2006.*

[5-23] T. Yang, Y. Xuan, D. Zemlyanov, T. Shen, Y. Q. Wu, J. M. Woodall, P. D. Ye, F. S. Aguirre-Tostado, M. Milojevic, S. McDonnell, and R. M. Wallace, "Interface studies of GaAs metal-oxide-semiconductor structures using atomic-layer-deposited HfO_2/Al_2O_3 nanolaminate gate dielectric," *Applied Physics Letters 91, 142122 (2007)*

[5-24] P. D. Ye, D. G. Wilk, B. Yang, S. N. G. Chu, K. K. Ng, and J. Bude, "Improvement of GaAs metal–semiconductor field-effect transistor drain-source breakdown voltage by oxide surface passivation grown by atomic layer deposition," *Solid State Electron., vol. 49, no. 5, pp. 790–794, May 2005*

[2-25] Fei Gao, S. J. Lee, and D. L. Kwong, “Enhancement mode GaAs metal-oxide-semiconductor field-effect-transistor integrated with thin AlN surface passivation layer and silicon/phosphorus coimplanted source/drain,” *J. Vac. Sci. Technol. B 27(1), Jan/Feb 2009*

[2-26] Fei Gao, S. J. Lee, Rui Li, S. J. Whang, S. Balakumar, D. Z. Chi, Chia Ching Kean, S. Vicknesh, C. H. Tung,and D.-L. Kwong, “GaAs p- and n-MOS devices integrated with novel passivation (plasma nitridation and AlN-surface passivation) techniques and ALD-HfO_2/TaN gate stack,” *International Electron Devices Meeting, 2006*

[5-27] Goutam Kumar Dalapati, Aaditya Sridhara, Andrew See Weng Wong, Ching Kean Chia, Sung Joo Lee, and Dongzhi Chi, “Characterization of sputtered TiO_2 gate dielectric on aluminum oxynitride passivated *p*-GaAs,” *Journal of Applied Physics 103, 034508 (2008)*

[5-28] Ming Zhu, Chih-Hang Tung, Yee-Chia Yeo, “Aluminum oxynitride interfacial passivation layer for high-permittivity gate dielectric stack on gallium arsenide,” *Applied Physics Letters 89, 202903 (2006)*

[5-29] Masamichi Akazawa, and Hideki Hasegawa, “Formation of ultrathin SiN_x /Si interface control double layer on (001) and (111) GaAs surfaces for *ex situ* deposition of high-κ dielectrics,” *J. Vac. Sci. Technol. B 25(4), Jul/Aug 2007*